TECHNICAL REPORT NO. 388

(THIRD ANNUAL REPORT)

ELECTROMAGNETIC STUDIES IN SHOCK PRODUCED PLASMAS*

By M. Abele
H. Medecki
K. Tomboulian

April 17, 1964

*This work has been sponsored by the Advanced Research Projects Agency (Ballistic Missile Defense Office) and technically administered by the Fluid Dynamics Branch of the Office of Naval Research.

GENERAL APPLIED SCIENCE LABORATORIES, INC.
MERRICK and STEWART AVENUES, WESTBURY L.I., N.Y. (516) ED 3-6960

Project 5246

Total No. of Pages - v and 105

Copy No. (17) of 25

TECHNICAL REPORT NO. 388

(THIRD ANNUAL REPORT)

ELECTROMAGNETIC STUDIES IN SHOCK PRODUCED PLASMAS

By M. Abele
H. Medecki
R. Tomboulian

Prepared for

Director
Advanced Research Projects Agency
Department of Defense
Washington 25, D.C.

ARPA ORDER No. 207-62
Contract No. Nonr 3475(00)

Title of Project

"Studies of the Electromagnetic Properties of Nonuniform Plasmas"

Prepared by

General Applied Science Laboratories, Inc.
Merrick and Stewart Avenue
Westbury, L. I., New York

April 17, 1964

Approved by: _____
Antonio Ferri
President

TABLE OF CONTENTS

TABLE OF CONTENTS (Contd)

LIST OF ILLUSTRATIONS

LIST OF ILLUSTRATIONS (Contd)

CHAPTER I

INTRODUCTION

An integral part of the work performed on this contract has been the development of a spatially resolving electron density microwave diagnostic technique useful in a range of electron densities infrequently explored by other investigators. This technique permits accurate spatial resolution in plasma gradients for electron densities, orders of magnitude below that possible, using a conventional microwave interferometer. After an initial calibration phase in which argon was the driven gas in the shock tube, this microwave technique has been used to measure electron densities and electron density profiles behind normal air shocks in the range of Mach number 8.5-11 and initial pressure conditions of $\sim$ 1 mm Hg. When the results of the measurements were compared with the values of electron densities predicted on the basis of the accepted semi-analytical rate chemistry program, an order of magnitude discrepancy was found. Specifically, the measurements indicate an electron density behind the shock which tends to the equilibrium value at a rate which is about an order of magnitude faster than the one predicted by the numerical calculations. Since the shock conditions where the measured discrepancy exists are relevant to the

150,000 ft. altitude range aerodynamic calculations, it is deemed pertinent to explore the reasons for the observed discrepancy. To this effect an extensive program of measurements has been initiated with different gas compositions and the sources of errors in the measuring technique and the interpretation of the results have been analyzed. The information presented in this report will not necessarily represent the chronological development of the experimentation, but rather a summary of the physical problem and the methods of solutions.

The second part of this report will deal with the properties of an electromagnetic wave propagating through a plasma with random or periodic spatial density variations. Of particular interest in this problem are the conditions when the plasma is "under dense" and the period of the spatial variation is about equal to the half wavelength or a multiple wavelength of the incident radiation. The experimental research for this part of the program has been severely handicapped by the inability to generate experimentally a plasma which has the required fluctuation properties and is amenable to an analytical evaluation. Some tentative results of this work will be presented.

CHAPTER II

THE FACILITY

SECT. A-1 INTRODUCTION

The explicit purpose of the following detailed description of the GASL combined shock tube and waveguide facility is to enable other investigators to duplicate any or all parts of this highly successful experimental arrangement. Since it is the details rather than the basic principles that are time consuming in the fabrication of such a facility, great effort will be made to present all salient features.

SECT. A-2 BASIC SHOCK TUBE

In this experimental facility, the driven section of the shock tube is also used as a circular waveguide. Because of this duplicity, some precautions must be taken as to the choice of material, the surface finish, and the method of connecting tubing sections.

A compromise material for the tube is seamless stainless steel pipe. While this material is certainly not the best electrical conductor as would be desirable from the waveguide point of view, it offers the advantages of strengh, machinability, corrosion resistance and availability. The stock material used for the driven sections of the shock tube were commercially available, extra heavy, three inch stainless steel pipe. This tube has a nominal inside diameter of 2.9" and outside diameter of 3.5".

Highly desirable from the waveguide aspect is that the tube's inner diameter be constant. For use as a shock tube, the inner surface should be smooth with no wall discontinuities at the tube section junctions. To satisfy these conditions, each ten foot length of pipe was reamed and honed by a specialist in this field. The resultant inside diameter for all four driven sections was measured to be 2.917" $\pm$ .001".

The problem of coupling the tube sections is summarized as follows: for use as a waveguide, good and complete electrical contact must be maintained at each junction, the sections should join with a minimum angle between their axes, discontinuities in the wall should be minimized, and the junction must be pressure and vacuum tight and mechanically strong. Also desirable is a connection that can be easily removed and reassembled, since the insertion of various test sections may be required at any junction. In addition, each section, should be able to be rotated and be locked independently. This requirement originates from the fact that the microwave radiation is polarized and both parallel and perpendicular measurements are sometimes desirable.

To satisfy these requirements, the coupling assembly shown in figure A-2.1 was devised. In this scheme, one end of each tube section is machined with a right hand thread and cylindrical surface concentric with the inner axis. On the other end of each section, a left hand thread, an identical cylindrical surface, and a partical "O" ring groove are machined. This "O" ring forms the seal between sections, and is held in place by the inner surface of the coupling nut. These are relatively simple machining operations.

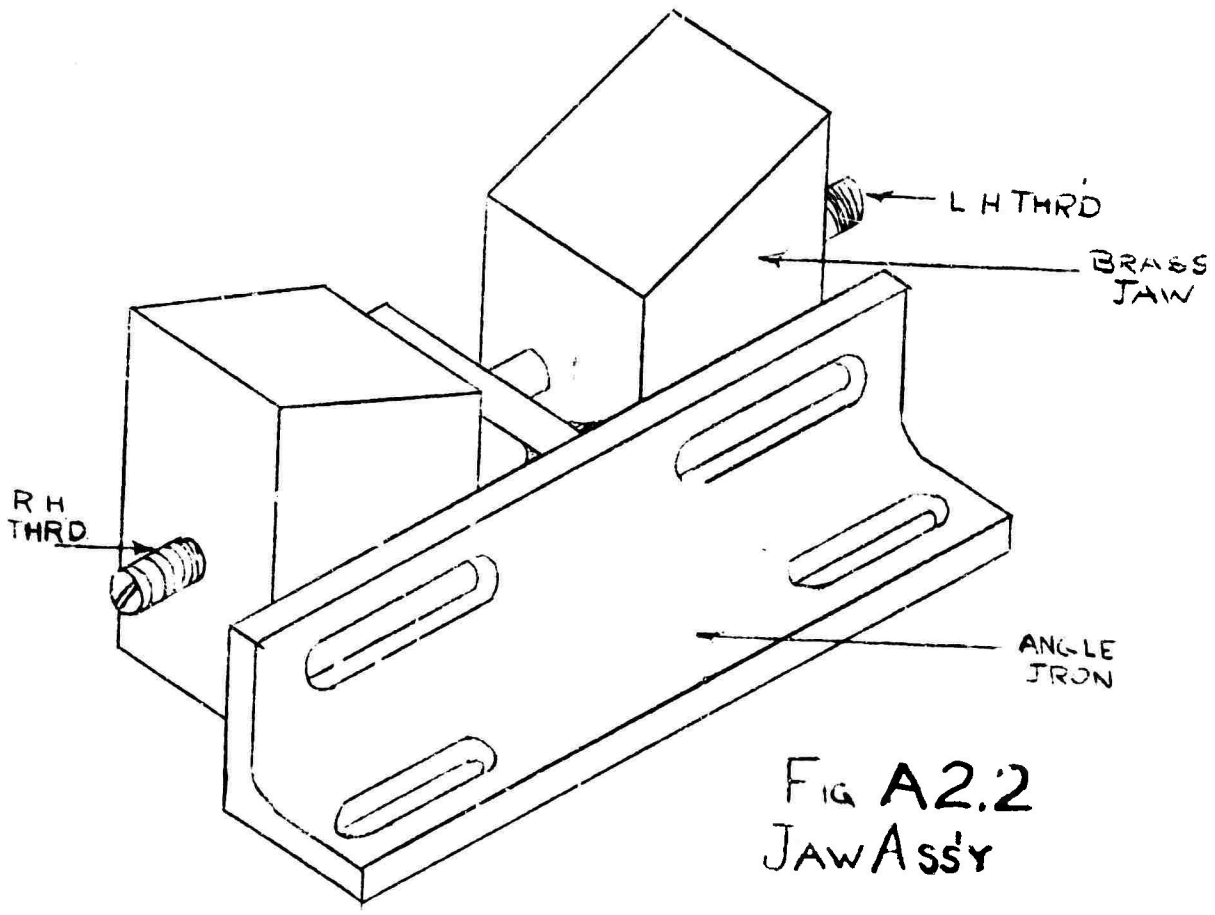

FIG A2.2
JAW ASS'Y

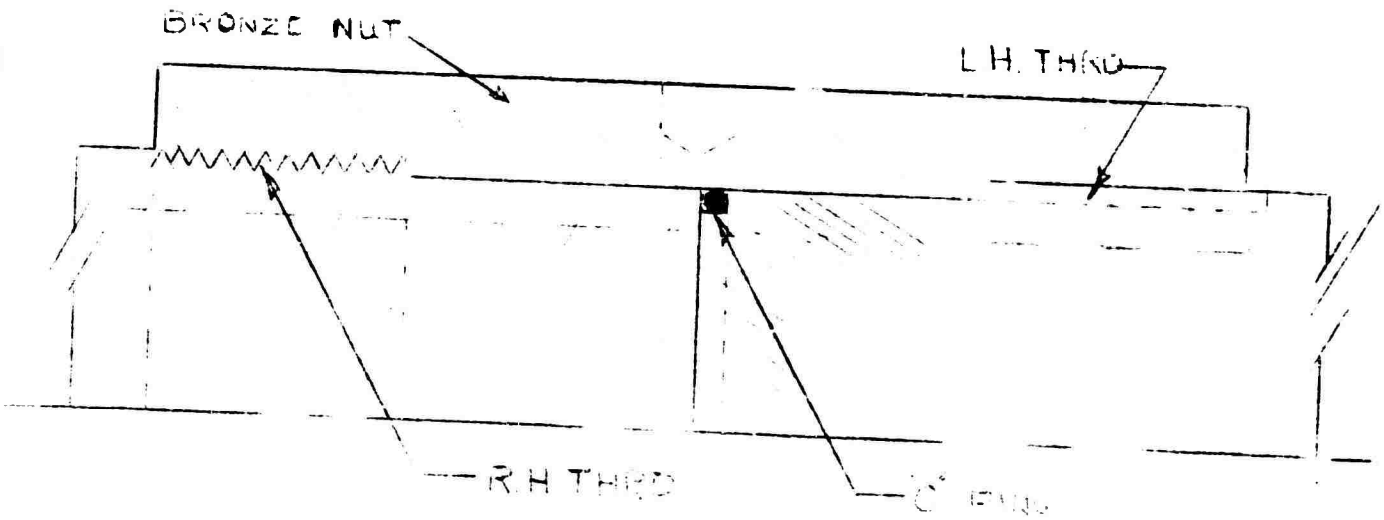

TYPICAL JOINT ASS'Y
FIG A2.1

and if done in the order stated, concentricity and diametric tolerances are maintained without the usual distortion problems associated with weld type coupling structures.

Bronze is used for the coupling nut to prevent galling of the surfaces, and is available as standard unfinished bronze bearing stock. If the tolerances of the cylindrical surfaces are held to .002", the maximum angular deviation between sections, excluding bending, is approximately .1 degree. Great care and patience should be exercised in the assembly of tube sections in order to prevent bending.

This coupling arrangement satisfies all of the conditions previously mentioned. However, in order to assemble and disassemble the tubes, the downstream sections must be able to slide on their mounting pads. Since the reaction forces on the shock tube exert only axial stresses, there is no need to rigidly restrain the tube along its length, so long as the main reactionary forces are absorbed at the diaphragm location. Since this is not only feasible but desirable from the point of view of simple electrical isolation from ground, the supports for the driven section need carry only the compressional weight load of the tube. This being the case, no extensive foundations or structure are required. Since perfect

alignment of these supports to the accuracy dictated by the coupling is not practically attainable, an adjustable set of "vee" jaws can be mounted on simple "I" beam structures to support the entire driven tube. Such a set of jaws are shown in Fig. A-2.2.

These jaws allow independent adjustment of height and horizontal position. The vertical adjustment is achieved by rotating the central screw which has right and left hand threads operating though the respective threads in the "V" jaws. The vertical load on the jaws is transmitted directly to the mounting plate on which they slide. Horizontal adjustment is made by moving the angle bracket, containing the center slot guide bearing, in the range provided by the slots in the bracket. The jaws are finally clamped to the angle bracket which is also slotted in the horizontal direction. Satisfactory support is accomplished with two sets of jaws for each ten foot section of tube. With this basic mounting and coupling arrangement the entire driven tube can be assembled in one day with the help of a precision level, an inexpensive transit, suitable "vee" blocks which will fit on the cylindrically machined part of the tube section, and a little patience and luck.

SECT. A-3 FAST OPENING MECHANICAL VALVE

General Characteristics

This valve has been developed and constructed to replace the diaphragm in a small shock tube.

The conditions of operation are:

Driver pressure	- 100 to 500 psi
Driver temperature	- up to 200°C
Opening area	- 7 sq. inches
Seal	- vacuum tight

Additional conditions which should be satisfied are remote operation and minimum of adjustment or replacement of parts. The adopted solution has only one moving part, a piston, that provides two types of seal: an "O" ring seal for vacuum and a sleeve valve for fast action.

Sequence of Operations

This sequence is shown in figure A-3.1.

(a) The valve is closed. Pressure in chamber A is equal to pressure in chamber B (driver). The resulting force pushes the piston towards the seal.

FIG. A-3.1

SEQUENCE OF OPERATIONS OF THE FAST OPENING VALVE

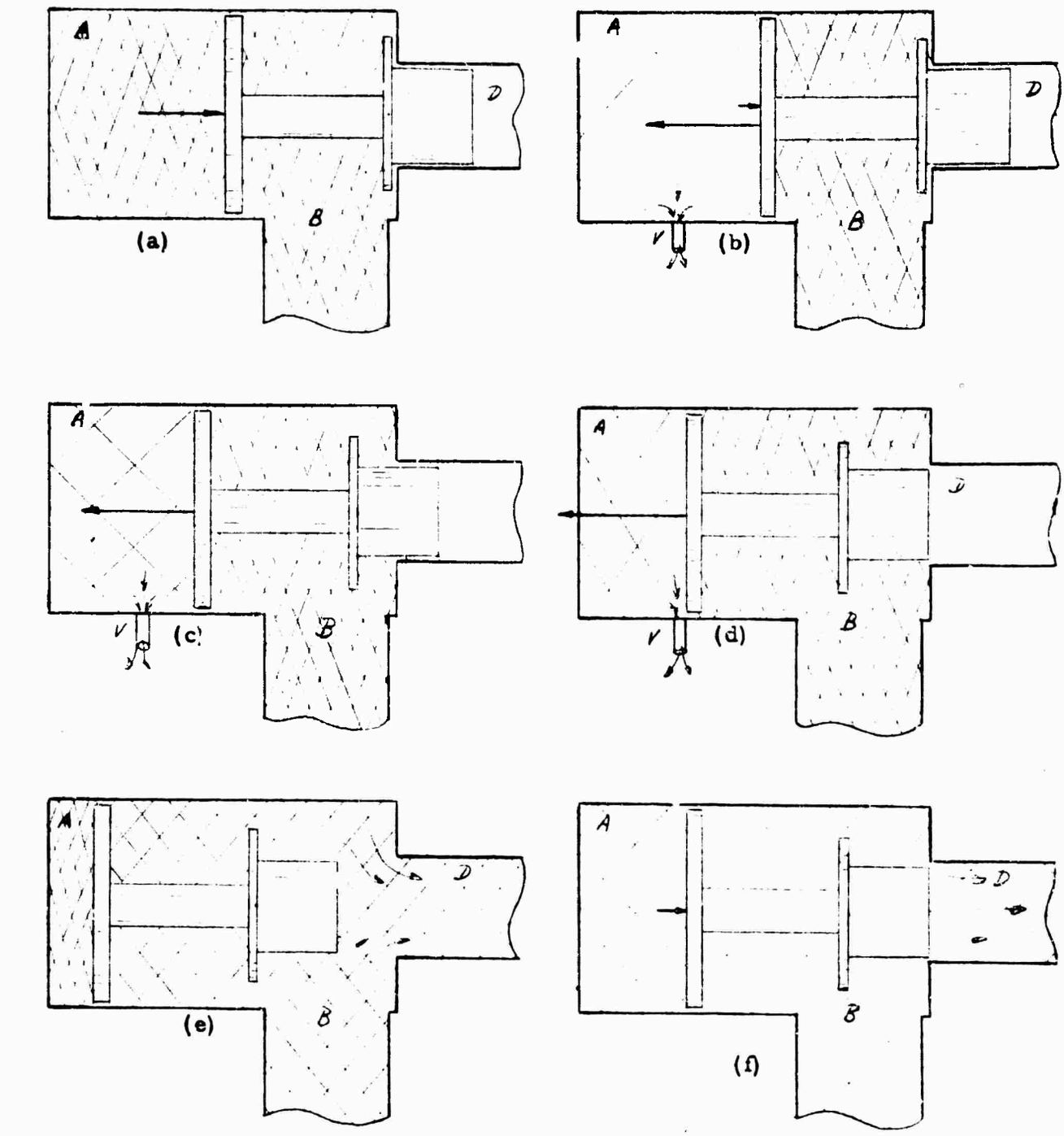

A CHAMBER

B DRIVER

D DRIVEN

V VENTING VALVE

C CHECK VALVE

H CHARGING VALVE

(b) Venting: Pressure in chamber A goes down towards atmospheric; the driver pressure remains constant. The resulting force pushing the piston drops and then reverses.

(c) Vacuum seal opening: When the piston starts to move towards the left the force pushing it increases suddenly because the pressure starts acting over the surface between vacuum seal and sleeve seal.

(d) Fast opening: When the sleeve goes out of the driver chamber the gas starts to flow from driver to driven. The piston has been accelerated along a distance equal to the length of the sleeve.

(e) Stopping: The piston compresses the gas left in chamber A, stopping and oscillating around a position which is a function of the final pressure of the tube.

(f) Closing: After firing,the driver and driven are evacuated: the gas left in chamber A expands and closes the valve.

(g) Charging: The gas is fed first into chamber A, closing the valve if step (f) fails to do so, and then the gas goes into the driver through a check valve.

The two main facts to be considered in the action of the valve are:

(1) The valve behaves as an unstable system near the firing pressure. The force pushing the piston jumps from zero to a maximum value in a very short time ($< 10^{-4}$ sec). This fast action cannot be obtained by controlling the flow of gas with conventional valves.

(2) The fast seal: Only after the piston receives its maximum velocity is the communication between driver and driven established. For a given acceleration of the piston the opening time goes down with the square root of the length of the sleeve.

The fast seal is not tight and the possible leakage between the opening of both seals establishes a compromise between length of sleeve, acceleration and quality of seal.

Computation of the Main Characteristics

The calculations are very easy if we disregard secondary effects.

The main parameters are:

S_A area of piston

S_B area of the vacuum tight seal

S_D transversal section of driven

P_A pressure in the chamber A

P_B pressure in the driver

W weight of the piston

e length of the sleeve

The pressure in the driven is , in normal working conditions, in the order of a few millimeters of mercury and we disregard it in the calculations. When charged it is $P_A = P_B$, and the force closing the seal is $F = P_B S_B$. The Chamber A is vented towards atmospheric; P_B remains constant and P_A goes down reaching the firing pressure P_f corresponding to zero force acting on the pist. $P_f = P_B (1 - \frac{S_B}{S_A})$; if P_f is equal to atmospheric pressure, the corresponding P_B is the minimum at which the valve can operate for a given ratio $\frac{S_B}{S_A}$.

When the piston starts to move, the force pushing it back jumps to $F_f = P_B (S_A - S_D) - P_A S_A$; because of the volume of the chamber A we can assume that $P_A = P_f$ during the fast seal

opening of the valve, so $F_f = P_B (S_B - S_D)$. With this force we can compute the acceleration, velocity and opening time.

We consider that the valve is open when the passage area of the gas through the fast seal equals the transversal area of the driven.

The corresponding values for the valve in operation are:

$P_f = 60$ psi.

$P_B = 300$ psi.

$S_A = 16$ in^2

$S_B = 13$ in^2

$S_D = 7$ in^2

$F_f = 1800$ pounds

opening speed = 120'/sec

opening time = 300 microseconds

Figure A-3.2 presents the calculated shock Mach numbers as a function of the pressure ratio between driver and driven for air. This calculation assumes an infinitely fast opening diaphragm and no energy loss mechanisms occurring in the flow. Experimental points (+) have been superimposed on the plot indicating the behavior obtained using the mechanical valve. The agreement equals or exceeds that obtainable using a bursting diaphragm.

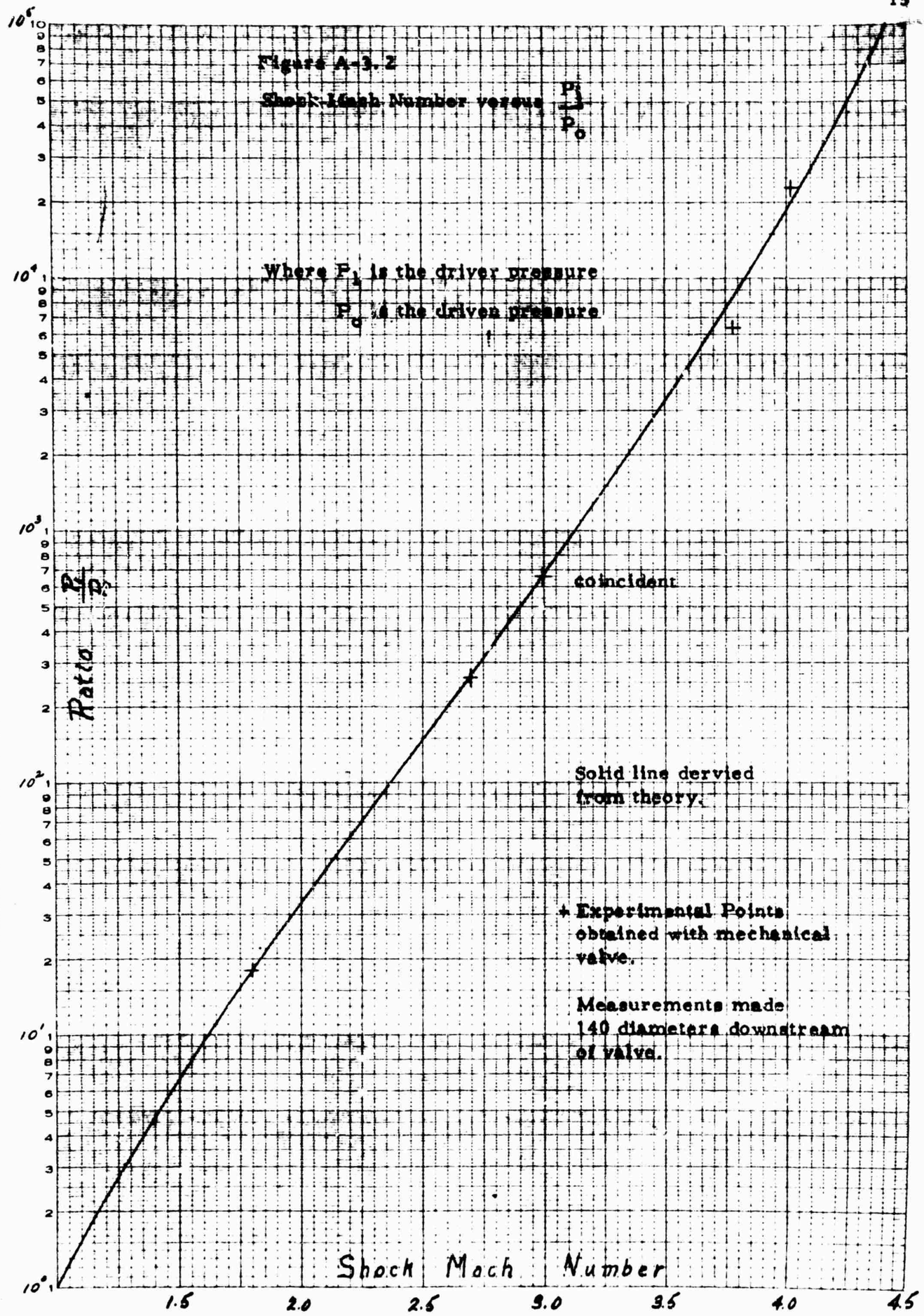
Figure A-3.2
Shock Mach Number versus $\frac{P_1}{P_0}$
Where P_1 is the driver pressure
P_0 is the driven pressure
Ratio P_1/P_0
coincident
Solid line dervied from theory.
+ Experimental Points obtained with mechanical valve.
Measurements made 140 diameters downstream of valve.
Shock Mach Number
1.5
2.0
2.5
3.0
3.5
4.0
4.5

Modifications

One modification refers to the elimination of the minimum firing pressure. The section S_A is equal to S_B, and the valve remains closed after the total venting of the chamber A. To fire, the chamber B is connected to the area $S_B - S_D$, initiating the motion; in this way, a better synchronization is obtained and P_A is lower, increasing the accelerating force.

The gas left in chamber A is not enough to stop the piston, so additional gas is injected after the valve is open. This is achieved with a bypass conduit which the piston uncovers on its way back during opening.

SECT. A-4 SHOCK TUBE PLUMBING

The governing factor in the engineering of the shock tube plumbing is safety. Since the driver gas normally used in the facility is hydrogen, the possibility of explosion either internally or externally due to a leak is omnipresent. While the basic tube is rated for over 1000 psi, the various detectors and fittings are in general not designed for these pressures. Hence, even a limited internal explosion is serious.

The replacing of the conventional diaphragm system with the mechanical valve has considerably reduced the hazards of operation. With the valve the use of the shock tube has become a closed operation. Since the tube need not be opened, the only air entering the system is introduced during the controlled filling cycle of the driven. This air charging can only be performed if the driver is not charged, the driven previously evacuated, and then the air charge cannot exceed on atmosphere. The driver cannot be filled until the pressure in the driven is again reduced below 50 mm Hg. Once the driver has been filled the only operation that can be performed is either "fire" or "purge". After firing, a pressure switch in the driven starts the purging cycle automatically, venting excess pressure over atmospheric to the atmosphere. Then the vacuum system is opened and the tube evacuated. While it is possible to bypass these automatic operations to obtain unusual conditions, it is generally during the routine

operation of such a system that a careless error is serious. Specific details of the plumbing system are not warranted here due to the fact that the use of the mechanical valve instead of a diaphragm has permitted additional simplifications. The basic system to be installed is outlined below.

The combined driver-mechanical valve as previously discussed need have only one solenoid type filling valve, and one small mechanical vacuum valve to be used only if the assembly is to be opened for cleaning or servicing. Another small solenoid valve may be used if the possibility of a high pressure dump is desired. The driven tube is equipped with two semi-automatic valves. The first is an over pressure valve which will seal vacuum but will open a two inch port if the static pressure in the driven exceeds one atmosphere absolute. This valve mechanically interlocks to the vacuum valve so that if the over pressure valve is open, the vacuum valve must be closed. The vacuum valve is pneumatically operated.

With this system a typical operating cycle would be as follows. The driven tube is pumped down by opening the pneumatic vacuum valve. The tube is filled with the desired test gas which is limited in pressure by the over pressure valve. The tube is now evacuated to the desired pressure. The driver is then filled. It may be noted that if the driver had

been inadvertently filled and fired during any of the above operations all systems including the vacuum pump would have been protected by the over pressure valve. When the firing sequence is started, a relay is locked so that the next pressure rise occurring in the driven will open the driven vacuum valve. After firing, if the pressure exceeds one atmosphere, the operation of the vacuum valve is blocked until a safe pressure in the driven is reached, after which the system will be evacuated leaving it in a safe condition and ready for the next test. For the above operation, it was assumed that the main mechanical valve operating in place of the diaphragm closed after firing. In the event that a malfunction occurs, no further operation of the shock tube is possible until the trouble is corrected, but neither are any safety problems present.

Two basic static pressure gauges have been found to be adequate in the system. To monitor the driver pressure a standard 250 psi Heiss gauge is used without valves or restricting orifices. An effective and accurate gauge for measurement of pre-firing pressure in the driven is the Alphatron gauge. This gauge (an old model) has three linear ranges, 0 100 microns, 0-1 mm. Hg., and 0-10 mm. Hg., with a zero shift raising the upper range to 20 mm. Hg. Supplementing the Alphatron gauge is a standard thermocouple gauge with one probe in the driven tube and another monitoring the pressure at the vacuum pump. Neither gauge

system is electrically damaged by operating at atmospheric pressure. So far, it has not been necessary to protect any gauge systems by isolation during firing. This is important from a safety standpoint, as well as an aid in avoiding possible readout errors.

SECT. A-5 VACUUM SYSTEM

A satisfactory range of initial pressures in the driven tube was deemed to be from 50 microns to 10 mm. Hg. To avoid the additional complication of a diffusion pump, a high quality, high capacity mechanical pump is used. Though pumping speed is slow near ultimate pressure, this range is seldom used for decontaminating the tube during firing. With the tube clean enough to avoid excessive gassing in the operating pressure ranges, the simplest and quickest way to achieve a contamination-free test gas is by repeated filling with test gas and evacuating. For instance, with the tube at atmospheric and full of hydrogen after firing, only two or three minutes pumping will evacuate it to .1 mm. Hg. By refilling with test gas and evacuating to test pressure, remaining hydrogen contamination is approximately only one part in ten thousand.

With the addition of a liquid nitrogen trap, the gassing contaminants important at low pressures (including pump oil) are removed. However, if the trap is used, a bypass system should also be employed since when pumping at high pressures, severe and wasteful boiling occurs in the trap. With the system tight, pumping for twelve hours with only the mechanical pump will reduce the pressure to a few microns. Using the trap, one micron can be obtained in two hours.

JECT. A-6 INSTRUMENTATION

The instrumentation discussed below are those devices and recording instruments pertinent to the general operation of the shock tube. The microwave instrumention is discussed in Section A-7. The specific problem under study requires a high degree of accuracy in all measuring and recording instruments. Three specific areas will be discussed; accurate location of the aerodynamic shock, measurement of dynamic pressures and recording of fast rise, small amplitude electrical signals.

Location of Shock Front

Accurate estimates of the equilibrium properties of the gas behind the incident shock can be made if the initial pressure and the shock velocity are known, the latter parameter being the most sensitive. Measurement of the shock velocity can be made by measuring the time interval between two points along the tube where an observable property associated with the shock front can be detected. The difficulty in this problem is the measurement of a property directly attributed to the shock front. Basically only three fundamental parameters are implicitly associated with the shock; a temperature change, a pressure change or a density change. Measurement of parameters induced, such as electron density and light radiation to locate the shock front, assumes that these

properties abruptly change across the front. This assumption is never strictly valid but may be satisfactory at high Mach numbers, when the use of ionization gauges or photomultipliers may be acceptable.

If it is desirable to detect the actual aerodynamic shock front, one of the fundamental property changes must be observed. A direct measurement of the density change can be made optically by measuring the deflection of a light beam. However, even for moderate strength shocks, this method is very delicate.

A direct measurement of pressure is possible except that the response time of the detector strongly limits the possible resolutions. That is, using a good quality crystal detector, a rise time of three microseconds is typical. If the shock velocity is on the order of 3 mm/ μsec (~M9), the spatial resolution is about 1 cm. Assuming the rise time is consistent for two gauges and the shock pressure profile is constant during the interval of the measurement, a velocity measurement is possible with a spatial resolution of .5 cm. Hence, to measure velocity to 1%, the distance between gauges should be .5 meters. It is clear however that for the purpose of locating the shock as a method of correlating events, the gauges have limitations. In addition, if measurements are to be made over a wide range of conditions, continual adjustment of sensitivity must be made. A more serious difficulty is the isolation of

the gauge from the mechanical shock generated when the diaphragm breaks (valve opens). If the mechanical shock reaches the gauge prior to the arrival to the aerodynamic shock, a spurious signal may render the measurement useless. A discussion of pressure gauges and measurements will be made in a following subsection.

Heat Transfer Gauges

A satisfactory solution to a detector for locating the shock front has been found to be a heat transfer gauge. The basic gauge is a thin film resistance thermometer element bonded to a glass slug. The gauge response is a function of not only the temperature, but also the density. This combined response allows the useful operation from M~4 to ~14 in this facility. The gauge is fabricated by painting a thin strip of metallic silver coating less than 1 micron thick and 1 mm. wide on a glass disk 1/4 inch in diameter. This film is then baked, and connecting leads are fed through two holes in the glass disc and soldered to the film. The entire front surface is then given a thin coating of magnesium flouride, which aids in preventing the collection of the charge diffused in front of the shock (Ref. 1). Unsatisfactory measurements are obtained without the coating. In operation, a steady current of 10-50 ma. is passed through the resistance element (thin film). The temperature change as the shock

passes, creates a change in resistance which generates a change in voltage if the current is nearly constant.

An extremely simple method of generating an essentially constant current is to use a large voltage with a large series resistor to the gauge as shown in Fig. A-6.1. To be sure, this system is wasteful of power, but its simplicity over a suitable transistor stabilized constant current supply for each gauge is obvious.

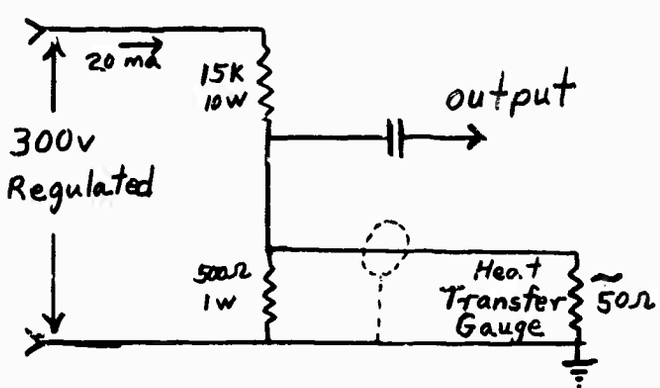

Fig. A-6.1
HTG Power Supply

To obtain a significant pulse (20 volts) from this circuit, very large amplification (20×10^3) of the voltage pulse must follow. If the fast response of the gauge is to be fully utilized, the amplifier should have a rise time of .3 μ sec.

To make the gauge useful as a standard and reliable shock front detector the circuit shown in Fig. A-6.2 has been designed and built. The circuit is intended to generate a sharp pulse and no attempt is made to preserve the long term (10 μ sec. or more) variations occurring at

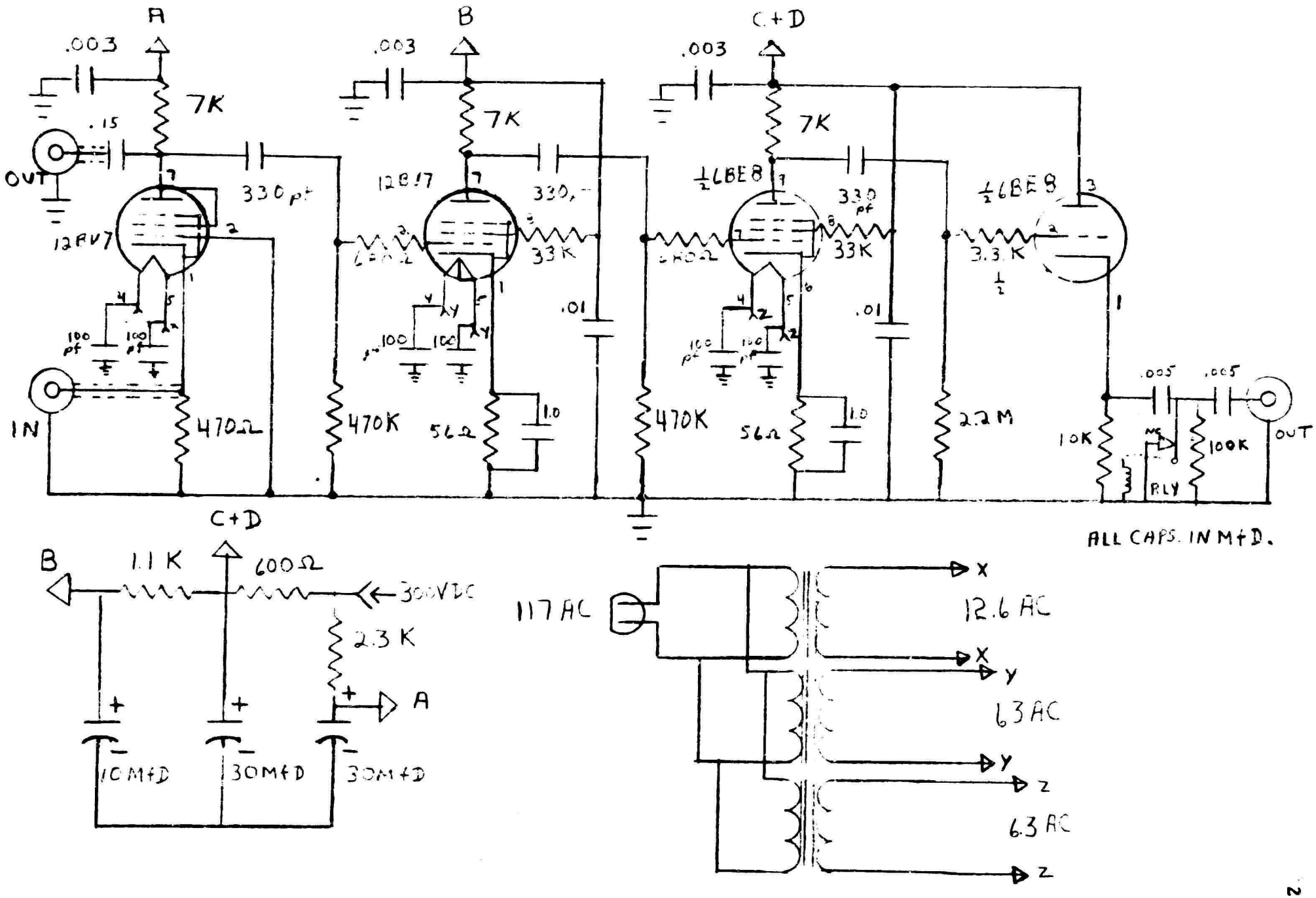

FIGURE A-6.2 - HTG Amp. Circuit

the gauge. That is, all the time constants are made conveniently small. The grounded grid first stage utilizes the low impedance character of the gauge to simultaneously provide a very stable first amplifier and the required bias current for the gauge element. The following two stages of amplification are conventional RC pentode amplifiers utilizing an extremely high transconductance tube. The output cathode follower allows extended cabling without loss of response time which is typically .3 microsec. The combination of series condensers and the normally closed relay in the final output provides a simple method of avoiding spurious trigger signals which occur from the various switching operations performed in the firing sequence. Because of poor grounding practices in other nearby facilities, a common failing in many laboratories, minor power line noises generated by switching transients are amplified by the high gain amplifiers. To minimize this problem, the first step in the firing sequence disconnects all unnecessary AC components from the system (fans, heaters, pumps, etc). The first step also applies a DC voltage to the time delay circuit of the output relay which opens a few seconds later. This system is not a replacement for proper grounding procedures but rather an insurance to avoid 60 cycle pickup and line transients.

Care must be taken in the general circuit construction because of the high gain. The general circuit construction utilizes Vector turret type sockets. Separate filament supplies are used as a precaution against high frequency oscillation. The separate transformers are practical if multiple units are to be constructed on the same chassis. For one amplifier unit one supply is probably adequate. The B+ supply can be unregulated with minor filtering. At 300 volts, the current consumption is about 70 ma. per amplifier. No gain control is used since in general the purpose is to provide a fast, large trigger. For most of the shock conditions shown in fig. B-4.5, the amplifier is saturated, thus generating a 60 volt, .2 microsecond rise time pulse, independent of shock conditions.

With this heat transfer gauge and amplifier, spatial resolution of the location of the front is comparable to the actual discontinuity in physical parameters occurring across the shock. Typically, this resolution is 1 mm, indicating that for a shock velocity of 3 mm/microsec. the required distance between detectors in order to determine velocity to 1% is about 10 cm, assuming the timer can resolve .3 microsec or better.

Pressure Detectors

Measurement of pressures or pressure variations behind the shock is extremely difficult if accuracy and space resolution are required. The only suitable gauge elements for this purpose are piezoelectric crystals. The basic problem in the design of a gauge for shock tube use is that the requirements of high natural resonant frequencies and high sensitivities are contradictory. The second problem is the design of the crystal mounting in the gauge so that the output is insensitive to external stresses at right angles to the measured stress.

If one considers that the useful pressure information in the shock tube occurs for an interval of a few hundred microseconds, there is a partial elimination of the measuring problems if a gauge intended only for dynamic purposes is used.

A precision calibrated crystal microphone with a natural resonant frequency of about 200 KC is the Massa model M-213. This microphone has good sensitivity and directional resolution, and can withstand severe overloads. A typical pressure trace using this microphone is shown in figure A-6.3. A low pass filter of RC constant 20 microseconds has been used to remove the initial ringing of the crystal, as shown in fig. A-6.4.

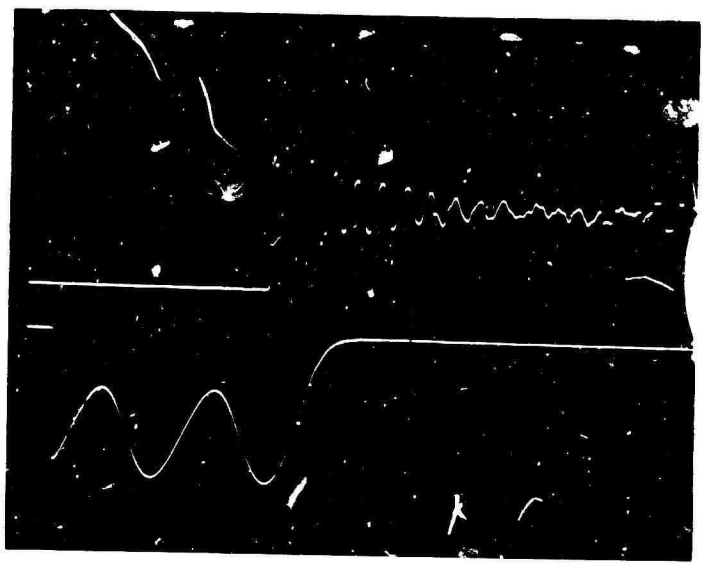

Upper Trace: Massa Microphone with no filtering - gain 15 db 5 volt/cm.

Lower Trace: Electric Field Detector - 50 mv/cm.

Sweep Time: 20 μs/cm.

Initial Pressure: 3 mm Hg - Air.

Shock Velocity: 3000 meters/sec.

Figure A-6.3

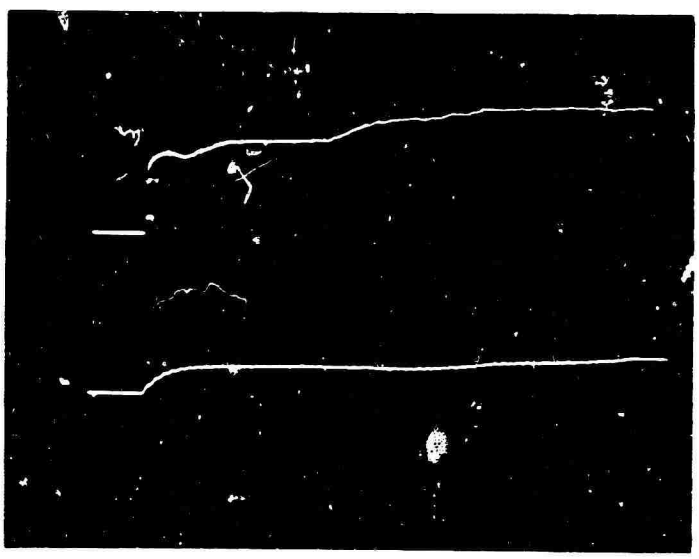

Upper Trace: Heat transfer gauge current 10 ma, 5 mv/cm.

Lower Trace: Massa Microphone with RC =20 μs filter - gain 20 db 5 volts/cm.

Sweep Time: 50 μs/cm.

Initial Pressure: 2 mm Hg - N_2

Figure A-6.4

Shock Tube Instrumentation, Typical Traces

Since this crystal microphone is only useful for dynamic pressure measurements, its calibration is difficult. In general the calibration supplied with the microphone is adequate. If doubtful, the microphone can be mounted in an inflated balloon, the pressure statically measured with respect to atmosphere, and the balloon punctured. The resultant step pressure change supplies a positive calibration point. Since the gauge and amplifier are relatively inexpensive, their use is strongly recommended if similar dynamic measurements are required.

SECT. A-7 MICROWAVE INSTRUMENTATION

Microwave circuit

The circuit is as shown in Figure A-7.1 includes a microwave signal generator (2-4 kmc, 60 mw), a coupling device delivering this signal to the shock tube, detectors of electric and magnetic fields, a recording system, consisting of oscilloscopes and photographic cameras, marker generators, wave shapers and delay generators. Sometimes a counter is used to measure the time between markers and consequently the speed of the shock.

The microwave signal generator is a reflex klystron with external tuneable cavity. This klystron is powered by a power supply which has the possibility to change reflector, grid and beam voltage. The frequency stability of this generator was good enough for our purpose, but the measurements being made were particularly sensitive to changes in the amplitude of the signal. Normally the klystron is switched on and off and the maximum tolerated short term change in the power output should be below 2%. Among the various methods tested, the one using negative pulses in the grid together with a Zener-stabilized bias power supply was found to be the most convenient.

Fig. A-7.1 Microwave and recording circuit

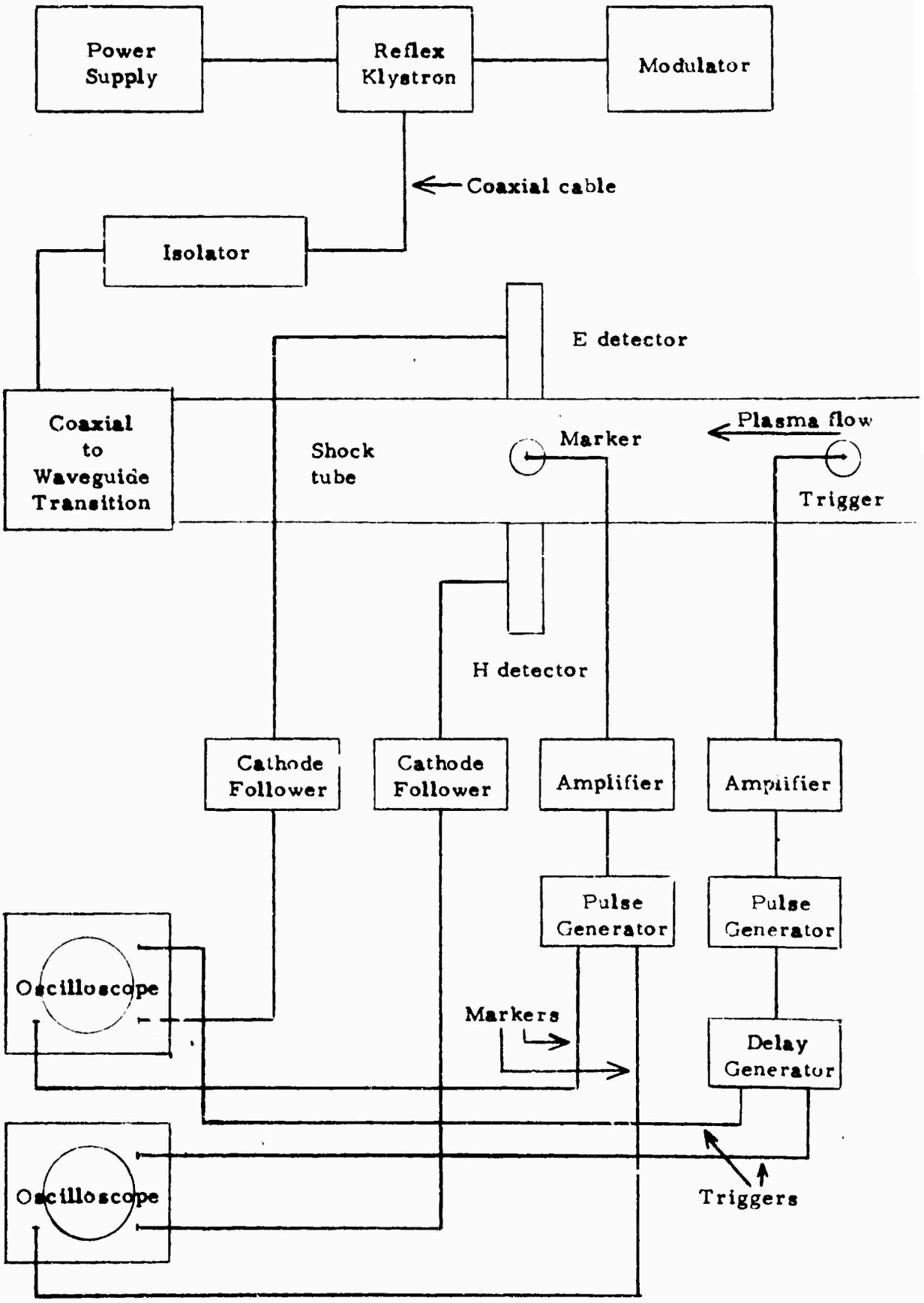

Coupling System

The output of the klystron is fed through an attenuator to a coaxial cable, an isolator, and from this to the coaxial waveguide transition. The shock tube equivalent to a circular waveguide operating in the TE_{11} mode. The coaxial to waveguide transition is shown in figure A-7.2. Matching is made by changing the penetration of the antenna and the position of the short circuit piston. The additional short circuit stub allows for adjustment of the bandwidth changing its length. The shocktube must be vacuum tight, and this is achieved by using a phenolic tube around the antenna and a bellows on the piston.

Matching

The matching of the coaxial line to waveguide is very important. All the measurements are based on the fact that the amplitude of the microwave signal coupled into the shock tube is constant. This condition is difficult to obtain because the plasma produces a strong reflection; standing wave ratio of twenty is not unusual. This reflected signal must be absorbed without reflection in the isolator. If reflections take place, they superimpose on the incoming signal with a phase that changes as the plasma moves. This effect is equivalent to a fluctuation of the input signal. The standing wave pattern then becomes a function of the position of the plasma or reflecting surface which is undesired.

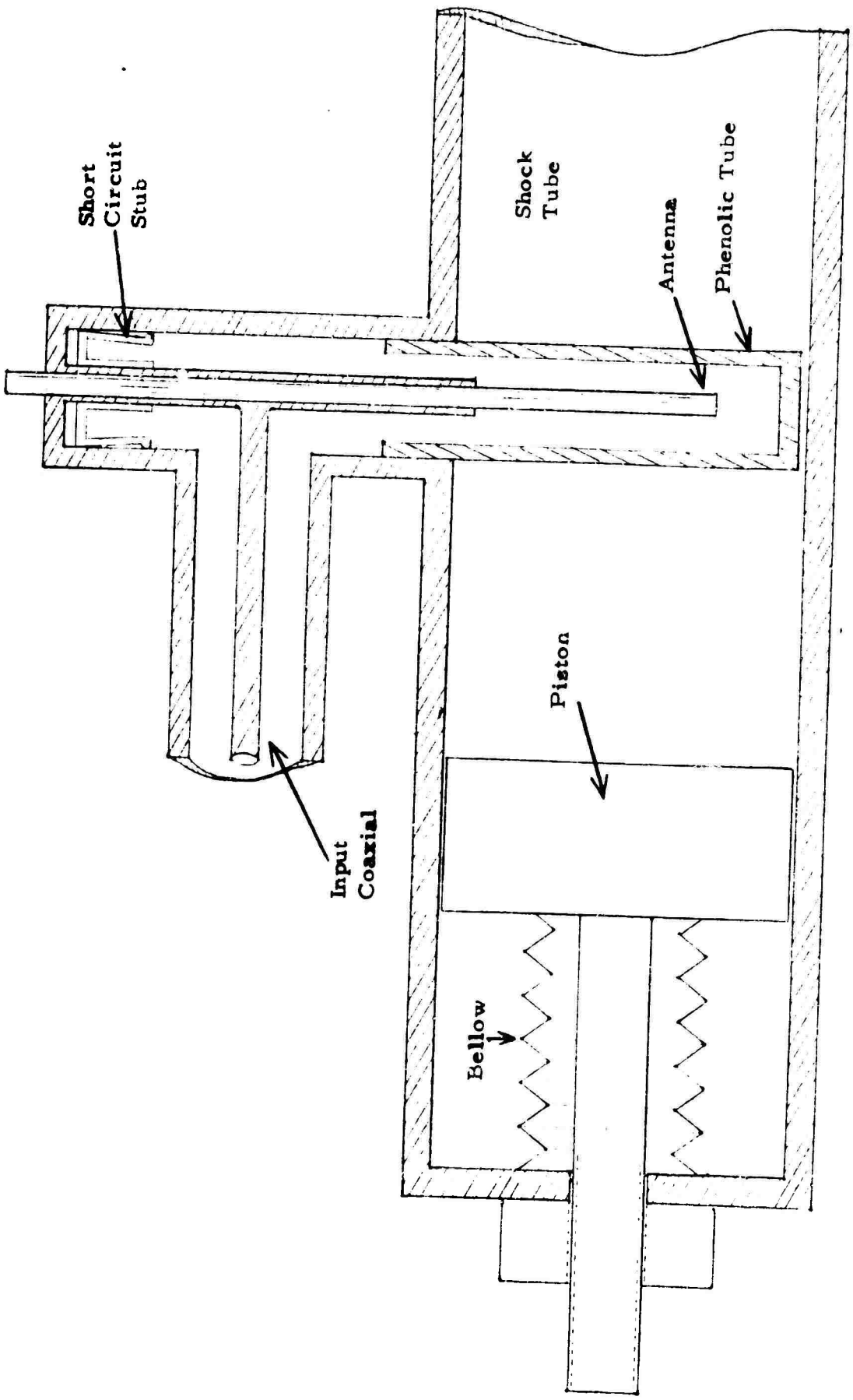

Fig. A-7.2 Coaxial to Waveguide Transition

Electromagnetic detectors mounted on the waveguide surface pick up the sum of both standing wave and fluctuation patterns, both having the same periodicity. A detector moving with the reflecting surface picks up the fluctuation only. The phase between the two patterns may take any value: if it is coincident with one, for instance E, the output from this detector will give a higher standing wave ratio than the output from the other. If the phase angle between the two patterns has any value the resultant pattern is not symmetric. In the computation of the plasma properties, it is assumed that the electromagnetic energy is perfectly coupled to the waveguide, hence perfect symmetry must be obtained to utilize the measurement.

Several methods have been used to get the desired matching but the only one actually used simple enough is the following. A short circuit piston is displaced along the shock tube, simulating a strong reflecting plasma. Moving with the piston is a detector picking up the magnetic field near the wall, where it is maximum. The output from this detector gives the fluctuation produced by the mismatch only. Successive adjustments of the antenna to waveguide transition are made attempting to eliminate this fluctuation, thus giving a constant output when the piston moves.

In order to reduce the frequency sensitivity of the antenna, the signal from the generator is altered slightly. The antenna short circuit stub is then adjusted until a minimum change occurs in the output of the piston detector during this frequency change.

The limit of this system of matching comes mainly from incomplete contact between piston and wall. A typical value of the fluctuation after the matching has been performed is 2%, but this corresponds to a smaller value when the plasma is reflecting the signal because of the significantly better reflecting properties of the metallic piston.

Detectors

The electromagnetic wave propagated inside the tube has a wavelength λ_g which is a function of the frequency, mode of propagation and diameter of the tube. Some of the radiating energy is reflected from the plasma and the ratio of reflected to incident power is a function of electron density, collision frequency and profile of the plasma. The combination of incident and reflected waves combines to form a system of standing waves along the tube. This pattern has a period of $\frac{\lambda_g}{2}$. When the plasma moves the pattern also moves with the same speed, provided the properties of the plasma remain constant.

A device detecting the electromagnetic field and located in a fixed position detects a signal whose amplitude goes from a maximum value equal to the sum of incident and reflected fields to a minimum equal to the difference between these two. For a plasma velocity v this fluctuation has a frequency $f_m = \frac{2v}{\lambda_B}$.

Two types of detectors have been used, one for the electric and the other for the magnetic field amplitude, as shown in figure A-7.3. The electric field detector is located in the region where it takes its maximum value, picking up the component parallel to the antenna and using a small, flush mounted surface in order to avoid introducing anything inside the shocktube which would disturb the flow. This surface is connected to a coaxial resonant circuit that matches impedances to the crystal detector and short circuits the currents produced by the flow of charges from the plasma to the tube walls. The magnetic field detector is a slot excited by the current flowing in the wall. Because of the relation between magnetic field and current this slot is equivalent to a loop located in a plane perpendicular to the slot. The field to be checked is the transversal component of H. The slot should be oriented in a transverse section of the tube and at the point where the electric field is maximum. The signal induced in the slot is coupled to a two line resonant circuit and to a crystal detector.

Electric Field Detector

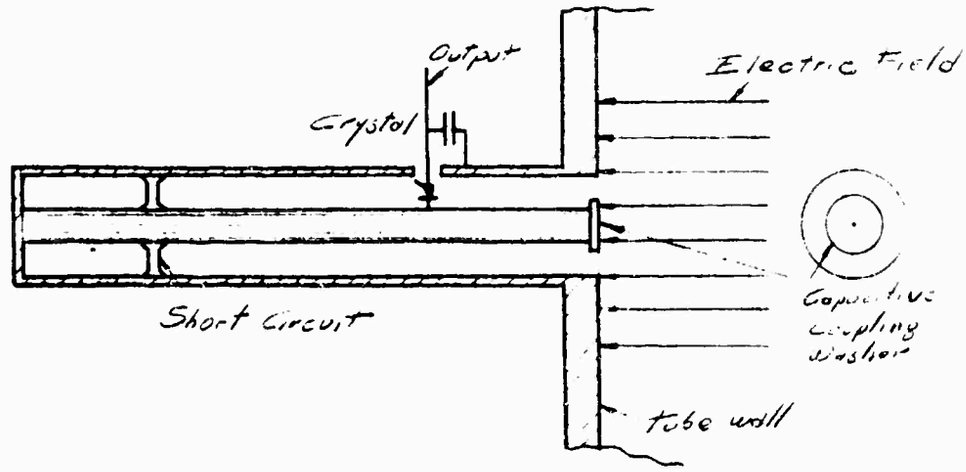

Figure A-7.3 (a)

Magnetic Field Detector

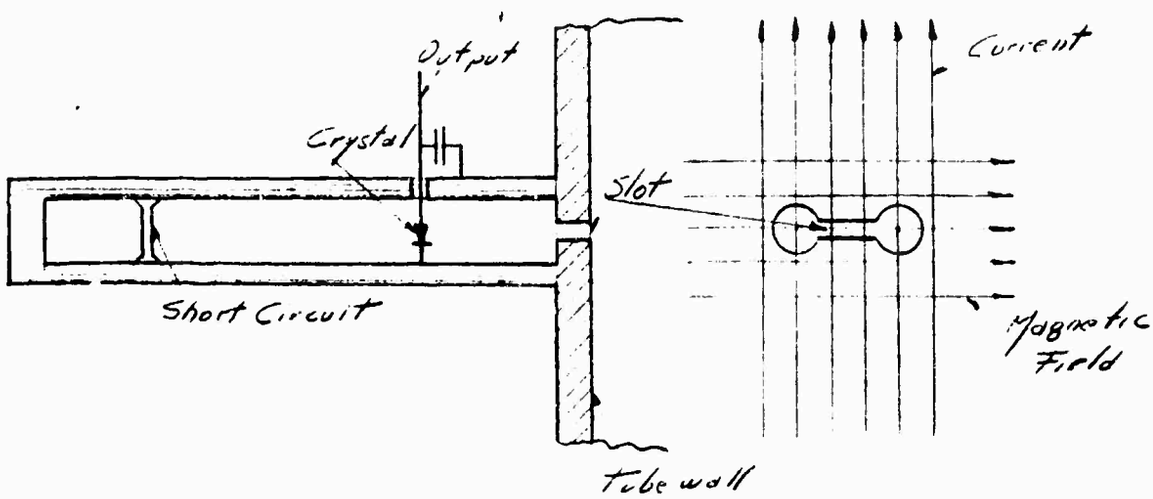

Figure A-7.3 (b)

For both E and H crystal detectors an output is obtained which is related to the amplitude of the respective field. The characteristics of the crystals cannot be considered linear nor quadratic and the required accuracy demands a calibration. The time response of the detectors is less than 10^{-7} sec if their output is directly connected to cathode followers. For simplicity's sake, AC amplifiers are used exclucively hence the DC level is not present. However, switching off the klystron gives this zero level reference, permitting the absolute amplitude determination from the single trace. The markers are equally spaced at known intervals providing a timing reference and a means of compensating for nonlinearities in the sweep.

To perform the calculation of the plasma properties the electric and magnetic fields should be determined in the same transversal section of the tube. A special section has been constructed allowing the placing of the two detectors plus a shock front detector in the same transversal section. In this arrangement, when the signal from one detector is maximum the other is minimum and vice versa. The oscilloscopes are triggered using various shock front detectors as discussed in section A-6.

SECT. A-8 DATA RECORDING

The only economically feasible method of recording analogue data consistent with shock tube time is the oscilloscope, although it is possible to record some data with video type tape recorders. However, the cost and resolution favor the oscilloscope and camera. While this basic technique is common-place, to achieve optimum fidelity of the data consistent with the errors in the system, each step of the process must be carefully analyzed. This error analysis is in many instances a function of the recording time. The range of interest for this facility are sweep times of from 5 microsec. to 500 microsec.

Two types of distortion can be delineated in the over-all process; these are amplitude and time distortion. To trace the source of these and estimate their relative and absolute magnitudes, the over-all recording process is divided into the following categories: the input amplifier up to the vertical deflection plates of the CRT, the sweep generator and horizontal amplifier up to the horizontal deflection plates, and the distortion in the CRT. Also, the photographic transfer of the CRT face, and the subsequent extraction of numerical data from the photographic traces must be considered. By far, the greatest offender in these distortion processes is that due to the CRT itself. While the

other factors are not always unimportant, each of the other parts of the process except numerical data reduction can be maintained to an order of magnitude better than the CRT distortion, if care is taken. Even with the best selected tubes, in order to obtain distortion levels on the order of .5% only the central region of the CRT screen can be utilized. Of course by so doing,this also tends to reduce all the other distortion causes listed. However, if these processes are independently investigated it becomes clear that the CRT is the arch criminal.

The specific procedure used to obtain the data for the shock electron density profile analysis discussed in section B-3 is outlined below. The critical traces were made using selected CRT's so as to minimize distortion. The photographic transfer of the trace was made using a modified scope camera to reduce the image size. Polaroid 10,000 speed film, extremely fast. enables the use of a small lens aperture. With this arrangement no distortion of a precision grid placed on the CRT was observable. The picture obtained was converted to a transparency by using a very small aperture on the enlarging lens. The subsequent transparency was enlarged in a 3" x 4" slide projector. In this projector, a 3/8" aperture was placed inside the standard lens assembly and a green filter was added to reduce chromatic

abberation. The resultant enlargement of about 12 diameters was negligibly distorted. The projection screen consisted of a layer of fine frosted glass backed by Plexiglass. The Plexiglass was precision scribed with .1" squares. The scribed lines were painted with phosphorescent paint. By using a "black lite" fluorescent behind the screen, the scribed marks were clearly visible, and direct transfer of numerical data from the picture could be taken by working from behind the screen. Such traces have also been made on large graph paper, but such paper is very often distorted, introducing significant errors. Under the best conditions, the overall error from amplifier input to data output was estimated to be .4% for the maximum values increasing to 2% for values 1/20 of maximum. The increase in error becomes significantly large for small numerical values because the trace cannot be resolved.

CHAPTER III ELECTRON DENSITY MEASUREMENT

SECT. B-1 ANALYTICAL FORMULATIONS FOR DETERMINING ELECTRON DENSITY

The following is a summary of the analytical expressions used to determine the electron density in the combined shock tube-waveguide. The polarized radiation is introduced in the downstream end of the tube. Probes to detect the radial electric field and the tangential magnetic field are upstream of the antenna, as described in Section A-7. To determine the point by point variations in electron density as the plasma moves past the detector station, expressions are required relating the measured field quantities to the local electron density.

For the TE_{11} mode of propagation, the radial electric field and the tangential magnetic field at the surface of the waveguide are given by,

$$E_r = A,\ J(\gamma,R) \cos\theta\, u(x)\, e^{i\omega t} \tag{1}$$

$$H_\theta = \frac{i}{\mu\omega} \frac{u'(x)}{u(x)} E_r \tag{2}$$

where γ for the TE_{11} mode is $\frac{1.842}{R}$, R being the tube radius.

The function u(x) is an undefined function which, however, contains the plasma properties. It must be a solution to,

$$u'' + u\left(\frac{\omega^2}{c^2} K - \gamma\right) = 0 \tag{3}$$

where primes indicate space derivatives, and ω is the radiating frequency, with

$$K = 1 + \frac{\omega_p^2}{\omega^2(1 - i\frac{\nu}{\omega})} \tag{4}$$

ω_p and ν being the plasma frequency and collision frequency respectively. Assuming the field components are measured at right angles, with the E_r field in the direction of polarization of the radiation, then

$$E_r = A_o u(x)\, e^{i\omega t} \tag{5}$$

$$H_\theta = \frac{i}{\mu\omega}\,\frac{u'(x)}{u(x)}\,E_r = \frac{i A_o}{\mu\omega}\,u'(x)\,e^{i\omega t} \tag{6}$$

Since the values of the fields that are measured, assuming a square law detection, are the square of the real parts of the respective field, the measured quantities are,

$$E_r E_r = A_o^2\, u(x)\, u^*(x) \tag{7}$$

$$H_\theta H_\theta^* = \frac{A_o^2}{\mu^2\omega^2}\, u'(x)\, u^*(x)' \tag{8}$$

where * indicates the complex conjugate. Solving for K^2 in Eq. (3),

$$K^2 = \frac{c^2}{\omega^2}\left[\gamma^2 - \frac{u''}{u}\right] \tag{9}$$

The solution of K^2 in terms of the field values of Eqs.(7) and (8) can be shown to be,

$$\text{Re } K^2 = c^2\mu^2 \frac{H_\theta H_\theta^*}{E_r E_r^*} - \frac{c^2}{2\omega^2}\frac{\left(E_r E_r^*\right)''}{E_r E_r^*} + \frac{c^2\gamma^2}{\omega^2} \tag{10}$$

and

$$\text{Im } K^2 = \frac{\left[\text{Re } K^2 - \frac{c^2}{\omega^2}\gamma^2\right]\frac{\left(E_r E_r^*\right)'}{E_r E_r^*} + c^2\mu^2\frac{\left(H_\theta H_\theta^*\right)'}{E_r E_r^*}}{\sqrt{4\omega^2\mu^2\frac{H_\theta H_\theta^*}{E_r E_r^*} - \left[\frac{\left(E_r E_r^*\right)'}{E_r E_r^*}\right]^2}} \tag{11}$$

The plasma properties in terms of Re K^2 and Im K^2 are given as,

$$\frac{\omega_p^2}{\omega^2} = (1 - \text{Re } K^2)\left[1 + \left(\frac{\nu}{\omega}\right)^2\right] \tag{12}$$

and,

$$\frac{\nu}{\omega} = \frac{\text{Im } K^2}{\text{Re } K^2 - 1} \tag{13}$$

The values of the field in the above equations are in MKS units. However, it may be noted that each field quantity appears in a ratio. All that is required for solution in terms of the nondimensional measured

quantities are the appropriate scaling ratios.

If the measured values of the field are designated as, E^2 and H^2, then the distance axis scaling needed for the ratios $\frac{(E^2)'}{E^2}$ and $\frac{(E^2)''}{E^2}$ can be determined from the ratio of the measured wavelength $\overline{\lambda g}$ (in units of the elongated trace). That is, if the horizontal (distance axis) coordinate is measured in units of Z and the real coordinate in X, units, then,

$$\frac{\overline{\lambda}_g}{\lambda_g} \equiv S$$

where λ_g is the actual waveguide wavelength (MKS units). Hence to scale the absolute ratios of field values to the measured quantities,

$$\frac{\left(E_r E_r^*\right)'}{E_r E_r} = S \frac{(E^2)'}{E^2}$$

and,

$$\frac{\left(E_r E_r^*\right)''}{E_r E_r^*} = S^2 \frac{(E^2)''}{E^2}$$

To scale the combined ratios of electric and magnetic fields, it may be noted that in the free space region, the ratios of the maximum field values (occurring 180° apart) is given by,

$$\frac{(H_\theta H_\theta^*)_{max}}{(E_\theta E_\theta^*)_{max}} = \frac{4\pi^2}{\mu^2 \omega^2 \lambda_g^2}$$

If the ratio of the same measured quantities is designated by (a), i.e.,

$$\frac{H^2_{max}}{E^2_{max}} = a,$$

then,

$$\frac{H_\theta H_\theta^*}{E_r E_r^*} = \frac{4\pi^2}{\mu^2\omega^2\lambda_g^2 a} \frac{H^2}{E^2} .$$

Then Eqs. (10) and (11) can be put in terms of measured quantities to give,

$$\text{Re } K^2 = \frac{c^2 4\pi^2}{\omega^2 \lambda_g^2 a} \frac{H^2}{E^2} - \frac{S^2 c^2}{2\omega^2} \frac{(E^2)''}{E^2} + \frac{c^2}{\omega^2} \tag{14}$$

$$\text{Im } K^2 = \frac{\left[\text{Re } K^2 - \frac{c^2}{\omega^2}\gamma^2\right] S \frac{(E^2)'}{E^2} + \frac{c^2 S 4\pi^2}{\omega^2 \lambda_g^2 a} \frac{(H^2)'}{E^2}}{\sqrt{\frac{16\pi^2}{\lambda_g^2 a} \frac{H^2}{E^2} - S^2\left[\frac{(E^2)'}{E^2}\right]^2}}$$

Hence, the plasma properties can be obtained through the use of Eqs. (12) and (13).

In summary, to calculate the plasma properties at any point behind the shock the following parameters are required.

λ_g	waveguide wavelength
$a = \frac{H^2_{max}}{E^2_{max}}$	taken in the free space region
$S = \frac{\bar{\lambda}_g}{\lambda_g}$	distance scaling ratios ($\bar{\lambda}_g$ measured wavelength on enlarged trace)
$\lambda = \frac{1.842}{R}$	R is tube radius
$\omega = 2\pi f$	f radiating frequency

and E^2, $(E^2)'$, $(E^2)''$, H^2, $(H^2)'$, the field values and derivatives at the wall of the waveguide.

SECT. B-2 DATA PROCESSING PROGRAM

In the preceding section describing the analytical formulation necessary for the electron density measurement, the basic quantities required for solution are the real value of electric field squared (EE^*), its first and second derivatives, the real value of magnetic field squared (HH^*), and its first derivative. It was shown that no absolute measurement of these quantities was required, if the ratio $\frac{EE^*_{max}}{HH^*_{max}}$ could be obtained in the free space region in front of the shock. The precision of the final calculation is extremely sensitive to these measured quantities. While it has been indicated in Section A-8 that the relative accuracy for part of the recorded data is about .4%, it is important to note that this accuracy is related to the data taken at that instant of time. Because all of the components of the measuring system are constantly varying, it is essential that all of the critical information be obtained from one set of traces taken at one time.

The greatest variables in this system are the crystal detectors, although sweep rates and amplifier gains may also change. If the desired signal to be detected is for instance EE^*, the crystal detector must have a square law behavior. Since this requirement is never precisely true a correction must be made on the output signal. It will be shown how this correction can be made directly from the numerical data derived from the single trace, thus avoiding the need for corroborating data taken at a

different time.

The calculation of electron density is divided into three operations. First, the raw numerical data taken from the scope trace is corrected for the non-square law behavior of the crystal. Second, from this corrected data, first and second derivatives are computed. Third, the corrected data and derivatives are combined point by point as prescribed by the analytic equations of the preceding section.

Processing of the Raw Data

The basic input for the calculation is approximately 150 data points from each of the raw electric and magnetic field detector output traces. These traces include one full period of the sinusoidal-like function preceding the plasma.

Because careless errors may be introduced in the transcription or punching of the raw data, the program first checks if successive points are monotonically increasing or decreasing. The object of this procedure is to identify data that is clearly impossible, and allow corrections or changes.

Once the data passes this initial test the points are smoothed by a least square fitting procedure. In this computation, eight points are used to obtain the constants of a second power equation by least squares fit. Having computed the equation constants, the values of the function for the

center two points are calculated and stored as smooth data. The program then jumps two points and recomputes the least square fit for the next eight points which of course includes six from the previous calculation. After this procedure has been performed for all data points, the initial raw data is destroyed and the smoothed values inserted in its respective place. The need for smoothing the data is comparable to the use of a "French" curve in graph plotting. The basic assumption is that the data is originally smooth and that conversion to digits has introduced a random error in the least significant place. By reducing these errors an improvement can be obtained in the subsequent derivatives that must be taken.

The next step is to modify the data for the incorrect response of the detector. This correction procedure is based on the fact that the data function outside the plasma must be a sinusoid if the detectors are measuring EE^*. The basic problem is to find a multiplicative function [g(x)] such that when multiplied by the data function [f(x)] the resulting function will be a sinusoid elevated above zero.

$$\text{i.e.,}\quad g(x)\, f(x) = A \sin \theta + A + \alpha$$

The difficulty in determining the g(x) function is that since α, which is related to the standing wave ratio, is unknown, then there are an infinite set of g(x) functions which will satisfy the above criteria. The solution to

this dilemma is found in the fact that the crystal nonlinearity (to the square law) must be a smooth and slowly varying function, a fact clear from the physics of the semiconductor. If α is on the order of A/3 or smaller, the latter condition becomes a very stringent limit on possible g(x) functions. The first step to determine the g(x) function is to determine the period of the sinusoidal like function f(x) in the free space region. This is accomplished by computing a function like a derivative over the entire curve. This derivative procedure consists of computing multiple differences at each point and averaging the result. The reason for this technique is to establish the zero slope points with the least error being introduced from the random data scatter.

After locating the first two zeros, forty points are generated by interpolation between zeros, which of course correspond to the first maximum and minimum or the reverse of the original curve. The forty points are chosen such that if the function were a true sine, then the increment of the function between points would be equal. This is done so that the g(x) function will not be unduly weighted by a preponderance of points at each end. The first trial g(x) function is generated by assuming the perfect sine curve has the same magnitude as the data function. Hence the g(x) function at maximum and minimum (A and B in Fig. B-2.1) is identically one. This then produces a g(x) typically like that in Fig. B-2.2. On the g(x) curve, the region from A to D, where D is arbitrarily 1/2 f(x),

is least square fitted by a second order polynomial. Point C, the value of g(x) for f(x) min. is computed from the curve fit constants and this value is used to compute the value of α .

Distorted Sine Function

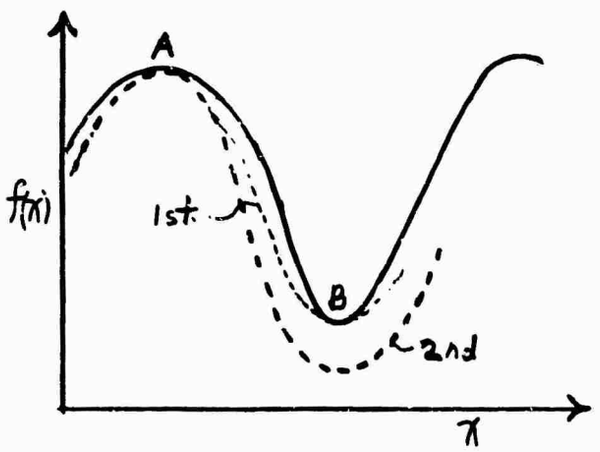

Fig. B-2.1

g(x) Determination

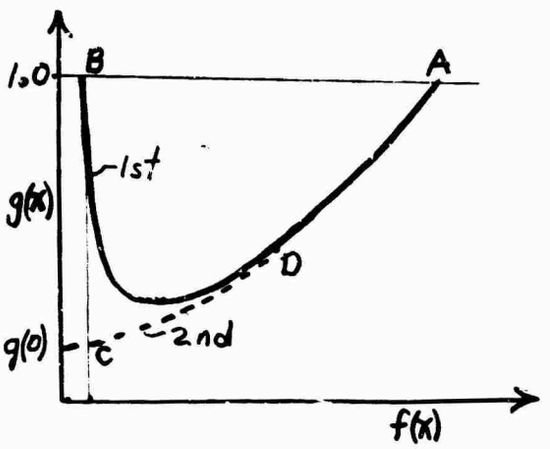

Fig. B-2.2

Using this value, a new magnitude A is computed and the entire g(x) function for each point of f(x) is generated. This second trial g(x) function is again curve fit to a second order polynomial by method of least squares. From the constants of the polynomial, the value of g(o) and the standing wave ratio are calculated and the difference between the curve fit g(x) and the trial computed g(x) points is printed. At this time in the proceeding, the computer is tired and returns control to the operator. The operator, making a human type judgment on the basis of the differences in

the last points may choose a different value by a few per cent of g(o) and the above process will be repeated.

It is desirable that the companion curve, HH^*, to the EE^* curve be processed up to the determination of the g(x) correction function as indicated above. If the g(x) functions have been properly chosen for each curve, the standing wave ratio will be identical. With a little practice the standing wave ratios can be made to agree to better than 2%.

Once the g(x) functions are satisfactorily determined, all the data is corrected thus yielding the "true" values of EE^* and HH^* along the curves. By a method of multiple differences, the derivative of these functions are taken yielding $(EE^*)'$, $(EE^*)''$ and $(HH^*)'$.

The computer program thus far described is intended to take data derived from a single trace, apply corrections and produce derivatives at fixed intervals. The functions generated must not only be self-consistent, but also should be consistent with the data derived from the companion curve. (EE^* and HH^* form a set) It has been shown how the program "forces" an overall amplitude correction by assuming the detected function in the free space region is sinusoidal. This type of correction will compensate for most amplitude distortions due to any cause that is not a function of the time coordinate (horizontal position on the CRT).

Additional information which can be obtained from the data is

the relative wavelength of the sinusoidal function in the free space region. It may be recalled that the wavelength determination was necessary to establish the period of the "forcing" sinus function. Since the waveguide wavelength of the microwave radiation can be accurately measured prior to testing, it is used as the only additional piece of information that is not directly obtained from the picture. If the measured wavelength and the relative wavelength are combined, an overall scaling is achieved. In addition, if the scaling factors for the EE^* and HH^* are compared, an accurate contraction or expansion factor can be obtained and used to provide exact time correlation between points on either curve. If one additional marker (such as the location of the shock front) is common to both curves an exact relation between the curves can be made. If the trace also contains time markers, the shock velocity can be obtained. It may be noted that the time markers also provide the location of the zero amplitude axis at the instant the trace was made, a procedure which removes the uncertainty due to drift in all systems.

An additional piece of information required for the calculation of electron density is the ratio of the maximum on the electric field trace in the free space region to the maximum on the magnetic detector trace $\frac{EE^*_{max}}{HH^*_{max}}$. This ratio provides all the scaling information needed to use the nondimensional curve data in an absolute determination of electron density.

It may be recalled that the maximum values required were obtained to provide amplitude information for the "forcing" sinusoidal correction function.

Hence, it has been demonstrated that the complete set of information required to compute the electron density, with the exception of the waveguide wavelength is directly obtainable from the two detector curves. The advantage of this procedure is that no absolute measurements are required, with the exception of the waveguide wavelength and interval between time markers. (The latter is used only for the velocity determination.) This clearly implies that no absolute calibration and maintenance of that calibration is needed for the instruments used in recording. Except for the requirement of a linear time scale (assuming shock velocity constant), an overall correction of most of the distortions occurring in all phases of the data collection process is obtainable from the data.

All of the information obtained in the "data processing" phase of the program is subsequently used in the point by point determination of electron density as per the formulations of the preceding section. Since this computation is entirely straightforward no discussion will be given here.

SECT. B-3 EXPERIMENTAL DETERMINATION OF THE ELECTRON DENSITY BEHIND A NORMAL AIR SHOCK

The following is a brief description of the experimental conditions for which the longitudinal electron density profile has been determined. A series of six independent sets of data have been processed corresponding to nearly identical shock conditions. The purpose of the nearly redundant data was to check the overall repeatability and the effect of small variations in shock condition about the mean.

The specific shock conditions are tabulated below.

Case	Shock Velocity (meter/sec)	Initial Pressure (mm Hg)	Note
1	3100	2.5	Upper curve
2	2900	1.5	Lower curve
3	3030	2.0	
4	3015	2.05	Mean values
5	3035	1.95	plotted
6	3020	2.0	

The velocities quoted above were calculated directly from the electric and magnetic field detector traces as previously described in section B-2. The microwave instrumentation used is described in Section A-7. The specific waveguide wavelength for all of the runs was 20.2 cm.

One typical set of traces is shown in Fig. B-3.1. Note the periodic time markers which also give the zero level of the signals. The location of the shock front was determined from a third trace.

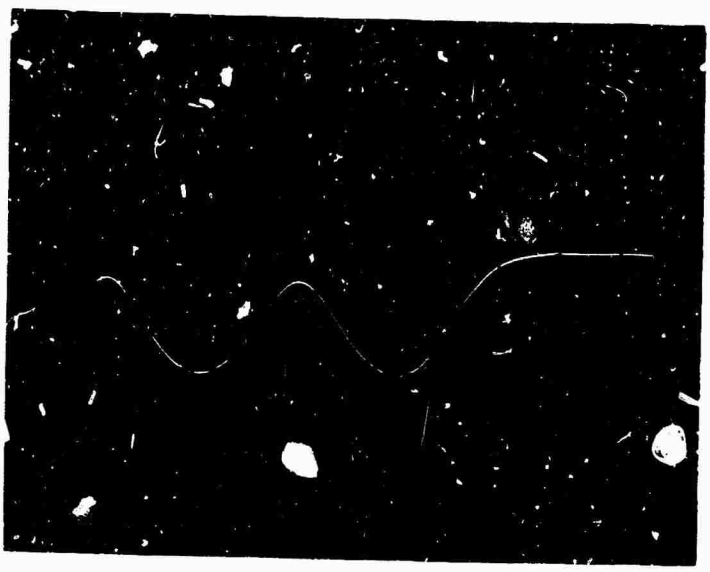

Electric Field Trace

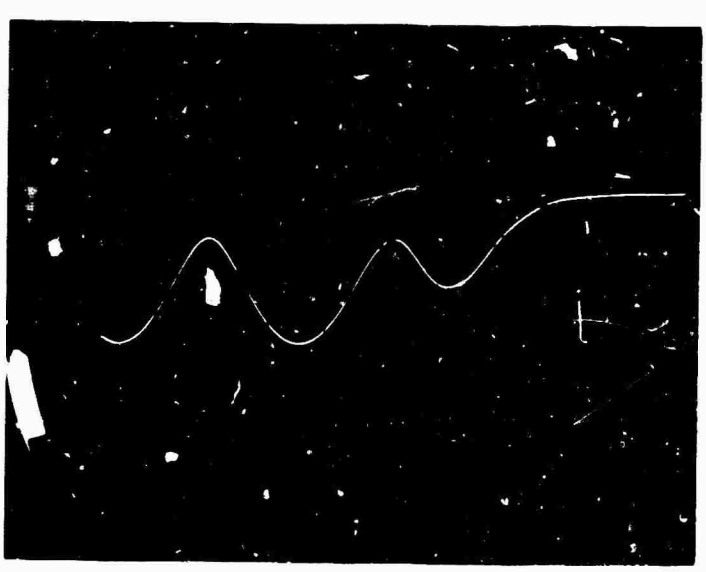

Magnetic Field Trace

Set of Electric and Magnetic Field traces used as starting data in the calculation of the electron density profile behind the shock. (Case 4 in table).

Figure B-3.1

The numerical data from these curves was obtained in the manner described in Section A-8. Subsequent numerical analysis was carried out using the computer program described in Section B-2. The results for the six cases are summarized in Fig. B-3.2. Here the mean curve represents the results for cases 3 through 6 which correspond to the same velocity conditions ±.3%. Cases 1 and 2 correspond to higher and lower velocities respectively. It may be noted that the behavior of the electron density is in correspondence with these conditions. The values of equilibrium electron density were calculated for these shock conditions using the procedure outlined in B-4 and Fig. B-4.2.

Because the shock front marker detector used in these runs was derived from a pressure detector as described in Section A-6, a small displacement uncertainty existed in the results consistent with the "jitter" of the relatively slow rise of the detector. The "mean" curve in Fig. B-3.2 represents a repositioning of the separate results, where the maximum shift corresponded to .75 cm.

The test gas for all of these cases was commercial compressed breathing air. The basic result has not been significantly modified by any of the following procedures.

(1) Addition of a liquid nitrogen "freezeout" trap on the test gas. Such a trap would of course remove all water and oil present.

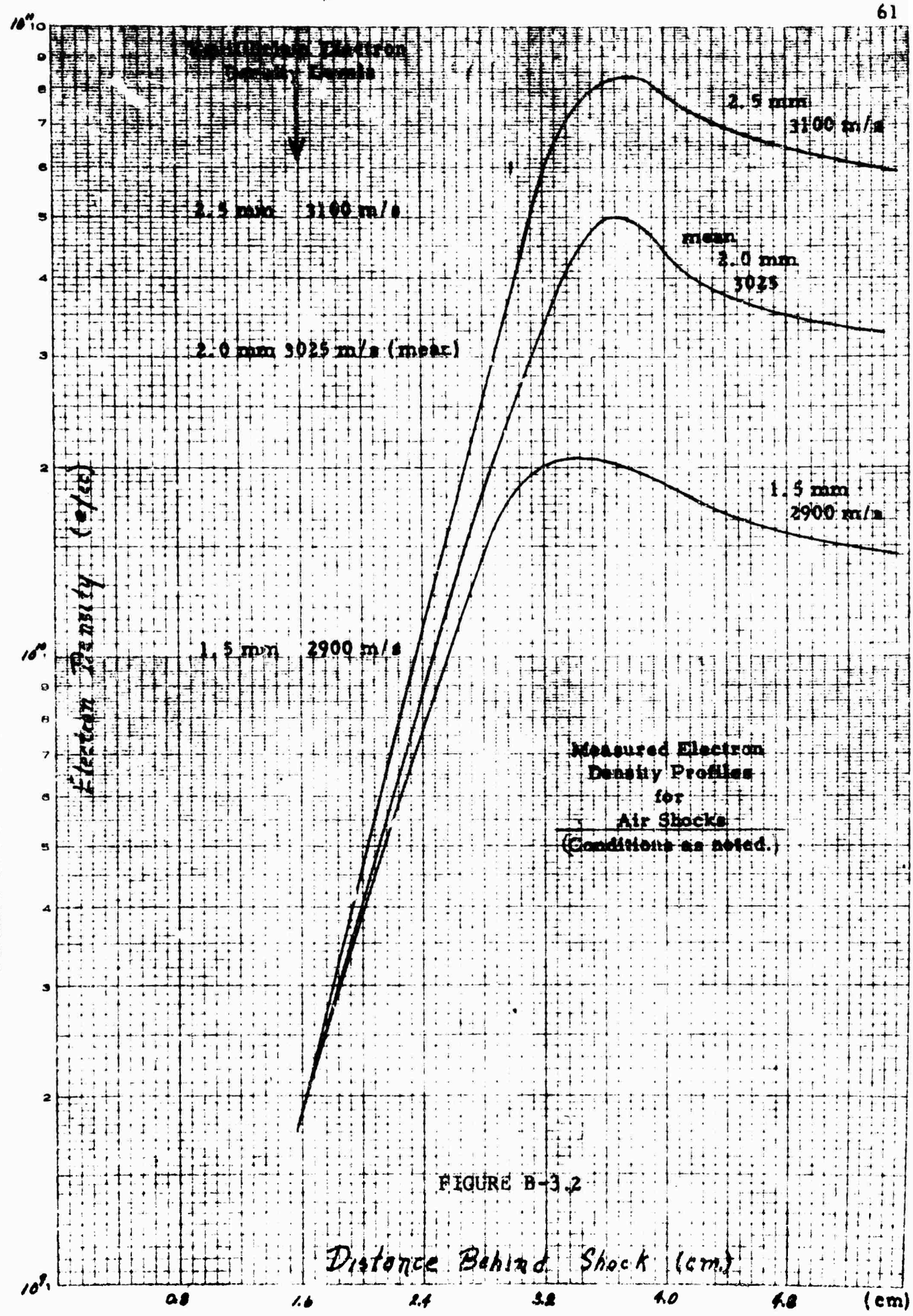
Electron Density (cm⁻³)
Distance Behind Shock (cm.)
(cm)
0.8
1.6
2.4
3.2
4.0
4.8
2.5 mm 3100 m/s
2.0 mm 3025 m/s (mean)
1.5 mm 2900 m/s
2.5 mm 3100 m/s
mean 2.0 mm 3025
1.5 mm 2900 m/s
Measured Electron Density Profiles for Air Shocks (Conditions as noted.)

FIGURE B-3.2

(2) Liquid nitrogen trap in the vacuum system to remove any trace of pump oil from the tube.

(3) Mixing of high purity oxygen and nitrogen in proportion to "normal" air and slight variation about the standard mixture. These gases were also liquid nitrogen trapped to remove water or oil.

(4) The design of the mechanical valve discussed in Section A-3 was motivated by the desire to remove the possibility of contamination due to the use of plastic diaphragms. However, no significant change of the electron density profile was observed after the conversion to the mechanical value.

Thus far, there is no indication of any type that the result obtained is not indicative of the electron density profile for the given shock conditions. Ultimately, the results from the spectroscopic analysis of the plasma region behind the shock as discussed in Section B-7 will determine if a significant impurity exists.

SECT. B-4 SUPPORTING INFORMATION

Radial Uniformity of the Plasma

One assumption made in the analysis of Section B-1 for the electron density was that of radial uniformity of the plasma density. Such uniformity can be altered by two factors. First is the presence of a boundary layer along the walls in the region behind the shock. However, for the penetration distances indicated by the results, this should have an insignificant effect on the assumption of uniformity.

The second effect is that of ambipolar diffusion. A calculation of this effect for two operating conditions has been performed as summarized in the following subsection. The result indicates the assumption of radial uniformity is basically correct.

Analytical Determination of Transverse Electron Density Profiles

The ambipolar diffusion equation for electrons in cylindrical coordinates is:

$$\frac{1}{r}\frac{\partial}{\partial r}\left(r\frac{\partial n_e}{\partial r}\right) + \frac{\partial^2 n_e}{\partial z^2} - \frac{u_n}{D}\frac{\partial n_e}{\partial z} + \frac{\dot{n}_e}{D} = 0 \qquad (1)$$

where $D = \frac{ukT}{M_i \nu_i}$ is the ambipolar diffusion. No Φ dependence of the electron distribution is included.

Only diffusion normal to the wall will be studied and for that particular case Eq. (1) becomes:

$$\frac{1}{r}\frac{d}{dr}\left(r\frac{\partial n_e}{\partial r}\right)+\frac{\dot{n}_e}{D}=0 \qquad (2)$$

The term, $\dot{n}_e$ which is related to the creation of electrons due to chemical reactions inside the ionized gas, as yet must be defined.

The mechanism for the creation of the electron is given by the motion of a shock wave along a tube. From the several reactions which can generate electrons in air due to the effect of the shock wave, the most important is:

$$N + O \rightarrow NO^{+} + e \qquad (3)$$

Therefore,

$$\dot{n}_e = k_r(K_c n_N n_O - n_e^2) \qquad (4)$$

Replacing (4) into (2) we have:

$$\frac{1}{r}\frac{\partial}{\partial r}\left(r\frac{\partial n_e}{\partial r}\right)+\frac{k_r}{D}(K_c n_N n_O - n_e^2)=0 \qquad (5)$$

Eq. (5) can be written in the form:

$$\frac{1}{r}\frac{\partial}{\partial r}\left(r\frac{\partial y}{\partial r}\right)+\frac{k_r n_{eo}}{D}\left(\frac{K_c n_N n_O - y^2}{n_{eo}^2}\right)=0 \qquad (6)$$

where n_{eo} is the equilibrium electron number density.

It is known from chemistry considerations (see Penner, Chemistry Problems in Jet Propulsion), that,

$$\frac{K_c n_N n_O}{n_{eo}^2} = 1 \tag{7}$$

Then Eq. (6) becomes:

$$\frac{1}{r} \frac{\partial}{\partial r} \left(r \frac{\partial y}{\partial r} \right) + \frac{k_r n_{eo}}{D} (1-y^2) = 0 \tag{8}$$

This equation has a boundary condition given by the following relation (see GASL TR-316, Chapter III).

$$\frac{D}{n_e} \frac{dr}{dr} = \sqrt{\frac{kT}{m_i}} \tag{9}$$

which can be written,

$$\frac{D}{y} \frac{dy}{dr} = \sqrt{\frac{kT}{m_i}} \tag{10}$$

The Eq. (8) with the condition (10) must be solved numerically and it has been done for 5 shock wave configurations. The data, corresponding to these configurations appear in Table I.

TABLE I

Shock Velocity	T	ρ/ρ_o	n_{eo}	α
m/sec	°K		cm^{-3}	cm
2750	2790	8.45×10^{-3}	4.4×10^{9}	1.404
3000	3000	1.00×10^{-2}	2.10×10^{10}	.639
3250	3210	1.08×10^{-2}	7.2×10^{10}	.348
3500	3390	1.22×10^{-2}	2×10^{11}	.204
3750	3660	1.30×10^{-2}	6.2×10^{11}	.120

Of primary interest is the effect of the coefficient,

$$\frac{1}{\alpha^2} = \frac{k_r n_{eo}}{D} \tag{11}$$

upon the electron distribution.

The coefficient α has the dimension of X length and can be considered to be a characteristic diffusion length. Table I shows that α changes greatly; it implying that for the cases where α is small, the diffusion will be very slow at the beginning but will fall off sharply near the wall of the cylinder. This does not happen for much higher values of α (see Fig. B-4.1). The experimental investigation made at GASL for a case where the shock wave velocity was 3100 m/sec corresponds to large values of α. For this velocity case, the transverse gradients are small

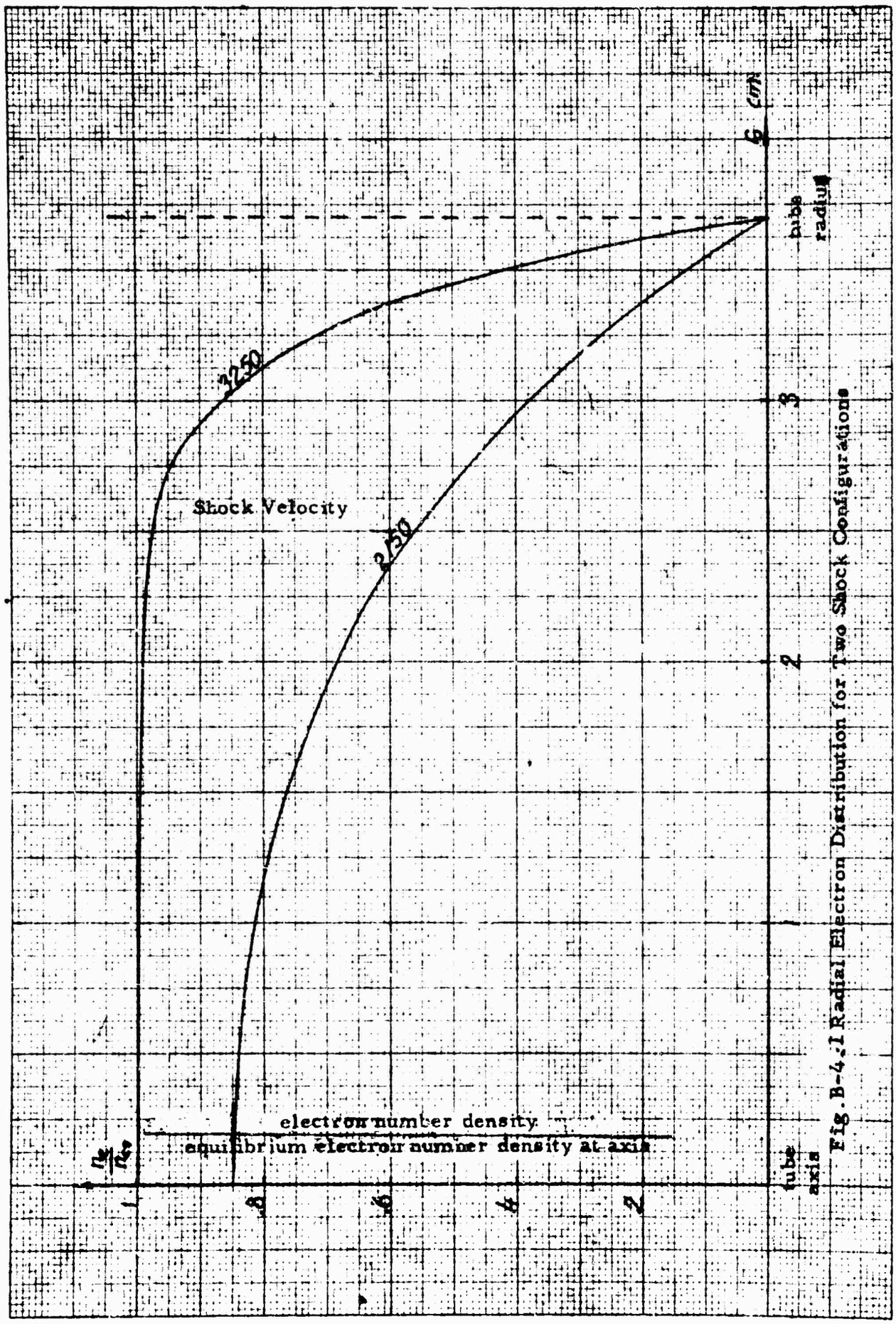

Fig. B-4.1 Radial Electron Distribution for Two Shock Configurations

over most of the tube radius, becoming large only in a thin outer sheath.

Sensitive Check on the Equilibrium Electron Density

By assuming a simple model for the plasma behind the shock to be a sharp transition from free space to equilibrium electron density levels, a formulation for the standing wave ratio due to the addition of the transmitted and reflected signals from such a plasma can be easily made.

By combining the formulation of the S.W.R. with the properties of the gas behind an air shock as a function of shock velocity and initial pressure, a comparison with experimental results can be made. This procedure is summarized below.

First, the standing wave ratio will be calculated in terms of the electron density and collision frequency which are assumed uniform in the plasma region.

The generalized propagation constant as defined by

$$\frac{d^2E}{dx^2} + K^2E = 0$$

is given by,

$$K = \sqrt{\frac{\omega^2}{c^2}\left[1 - \frac{\omega_p^2}{\omega^2(1 - i\frac{\nu}{\omega})}\right]} - \nu^2$$

where, ω is the propagating frequency

ω_p the plasma frequency

ν the collision frequency, and

γ is the root of the Bessel function for the TE_{11} circulator waveguide mode divided by the tube radius.

The propagation constant can be formed as follows. Define

$$K = k_o K_g$$

where

$$k_o = \sqrt{\frac{\omega^2}{c^2} - \gamma^2}$$

$$K_g = \sqrt{1 - \frac{\omega_p^2}{c^2 k_o^2 (1 - i\,\frac{\nu}{\omega})}}$$

Now let the radial electric field and the tangential magnetic field in the free space region be given by

$$E_r = A\, e^{-ik_o x} + B\, e^{-ik_o x}$$

$$H_\theta = k_o \sqrt{\frac{\epsilon_o}{\mu_o}} \left[A\, e^{-k_o x} - B\, e^{ik_o x}\right]$$

and in the uniform plasma region,

$$E_r = C\, e^{ik_1 x}$$

$$H_\theta = k_1 \sqrt{\frac{\epsilon_o}{\mu_o}} \left[C\, e^{-ik_1 x} \right]$$

Normalizing A ≡ 1, the boundary conditions are matched yielding,

$$E_r = e^{-ik_o x} + \theta\, e^{ik_o x}$$

with

$$\theta = \frac{1 - K_g}{1 + K_g}$$

Thus, the real component of the field produced is,

$$E_r E_r^* = 1 + \theta\theta^* + \theta\theta^* e^{-ik_o x}\, e^{ik_o x}$$

This is reduced to,

$$E_r E_r^* = \left[1 \pm \sqrt{(R_e\theta)^2 + (I_m\theta)^2} \right]^2$$

The two solutions give the maximum and minimum values. Thus the standing wave ratio is,

$$SWR = \left[\frac{1 + \sqrt{(R_e\theta)^2 + (I_m\theta)^2}}{1 - \sqrt{(R_e\theta)^2 + (I_m\theta)^2}} \right]^2$$

where θ is a function of ω_p and ν.

By solving the normal set of aerodynamic equations and using a programmed Mollier diagram, the conditions behind the shock can be

given as a function of shock velocity and initial pressure.

To simplify the calculation of equilibrium electron density from temperature and density, standard tables were programmed f the computer. Thus as a function of shock velocity, the equilibrium electron density is computed with the initial pressure as a parameter. Figure B-4.2 shows this plot. The collision frequency is computed from the approximation

$$\nu = \frac{5 \times 10^{12} p}{\sqrt{T}}$$

with p the pressure in atmospheres, T in °K.

If now these plasma properties are used to compute K_g, the standing wave ratio can be calculated using the previous formulation as a function of shock velocity with the initial pressure as a parameter (Fig. B-4.3). Hence as a function of accurately determinable quantities, the electromagnetic characteristics of the entire system can be computed and subsequently compared with the experimental quantities.

It should be appreciated that such a comparison is a very sensitive check on the assumptions made. First, the aerodynamic properties behind the shock must precisely follow the gas dynamic theory. Second, the electron density and collision frequency must, on the average, be identical with the equilibrium values. Third, the assumed geometric uniformity of the plasma region must be nearly correct. Fourth, the

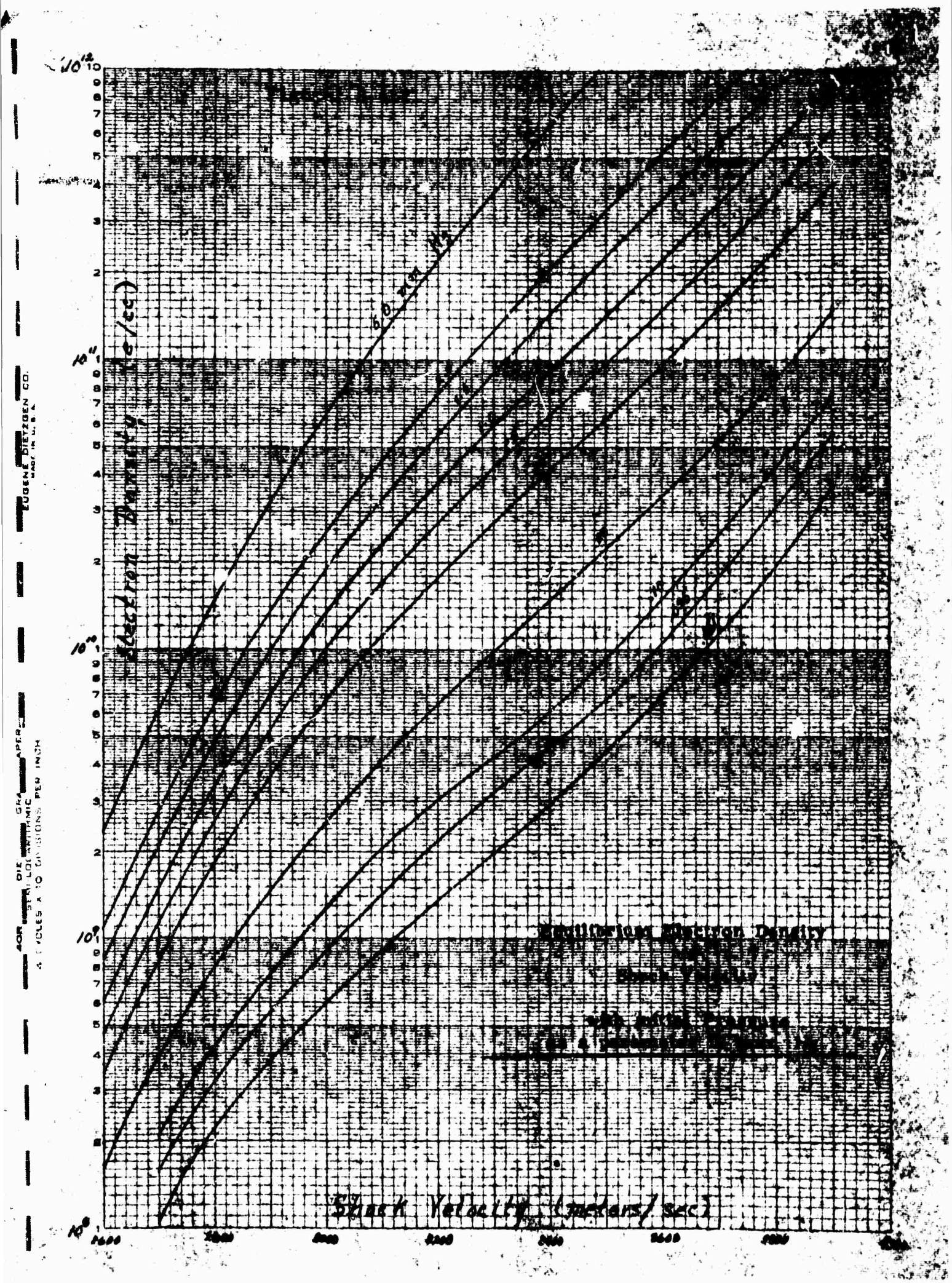
Electron Density (e/cc)
Equilibrium Electron Density
Shock Velocity
Shock Velocity (meters/sec)

Figure: B-4.3

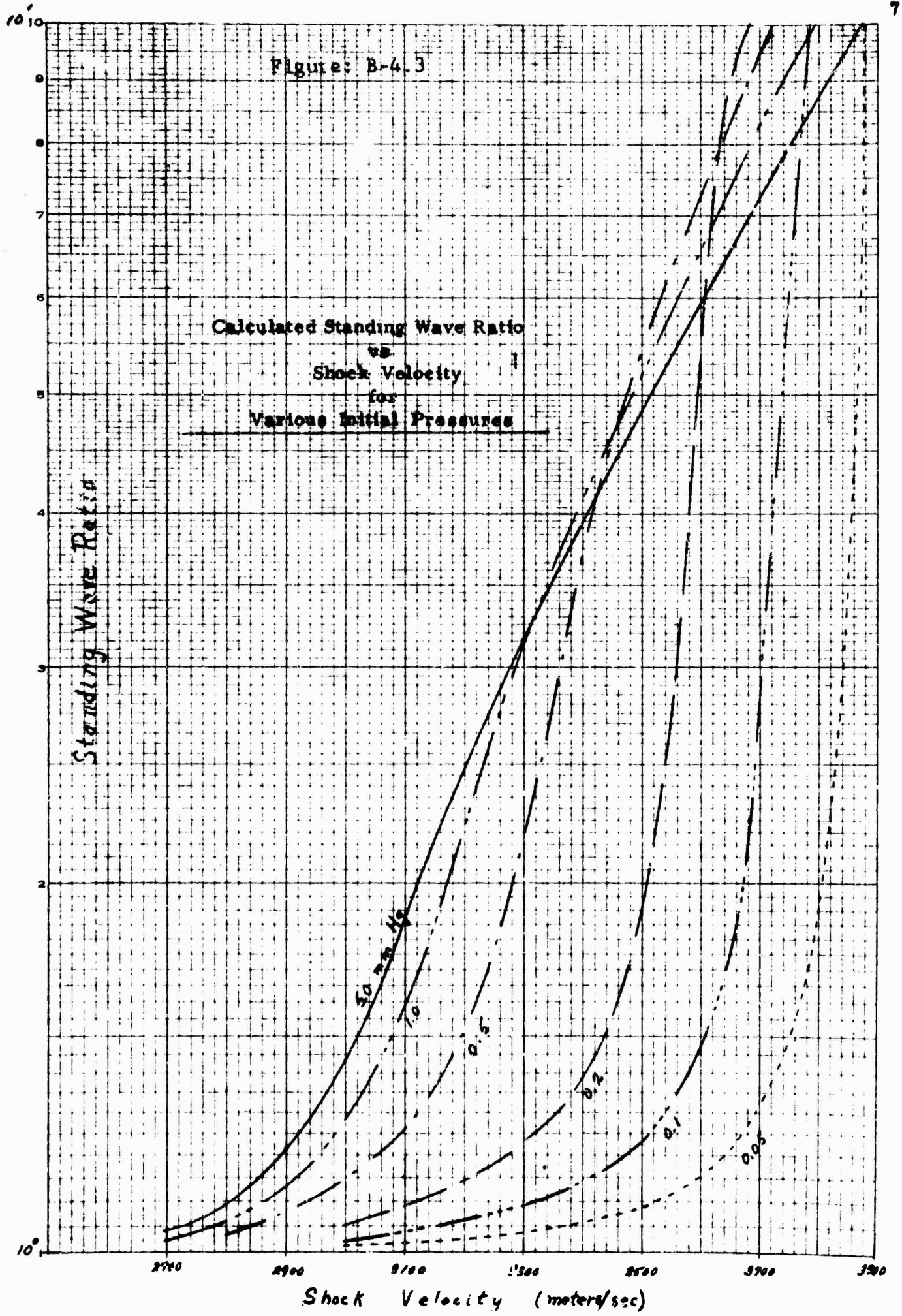
Calculated Standing Wave Ratio
vs.
Shock Velocity
for
Various Initial Pressures
Standing Wave Ratio
Shock Velocity (meters/sec)
50 cm Hg
1.0
0.5
0.2
0.1
0.05

calculation of the SWR based on the simple step model should be right. When comparing with experimentals, the variables measured must be identically the same as those used in the formulation. For instance, the electric field detector after correction should indeed be measuring only EE^*.

In this light, the correspondence between the analytically determined and the measured SWR as presented in Fig. B-4.4 is remarkable. Note here that since the driver pressure is constant for all these tests, in order to change the shock velocity there is a corresponding change in initial pressure. Hence, Fig. B-4.4 corresponds to a cross plot of Fig. B-4.3 using the operating characteristic curve in Fig. B-4.5. While by itself this agreement provides probable verification of the assumptions made, in conjunction with the electron density profile measurement discussed in Section B-3, the measurement provides strong proof that the point by point technique is indeed measuring the ionization relaxation length behind the shock.

Figure: B-4.4

Standing Wave Ratio
vs
Shock Velocity

(following actual operating conditions of shock tube. (See Fig. B-4.5)

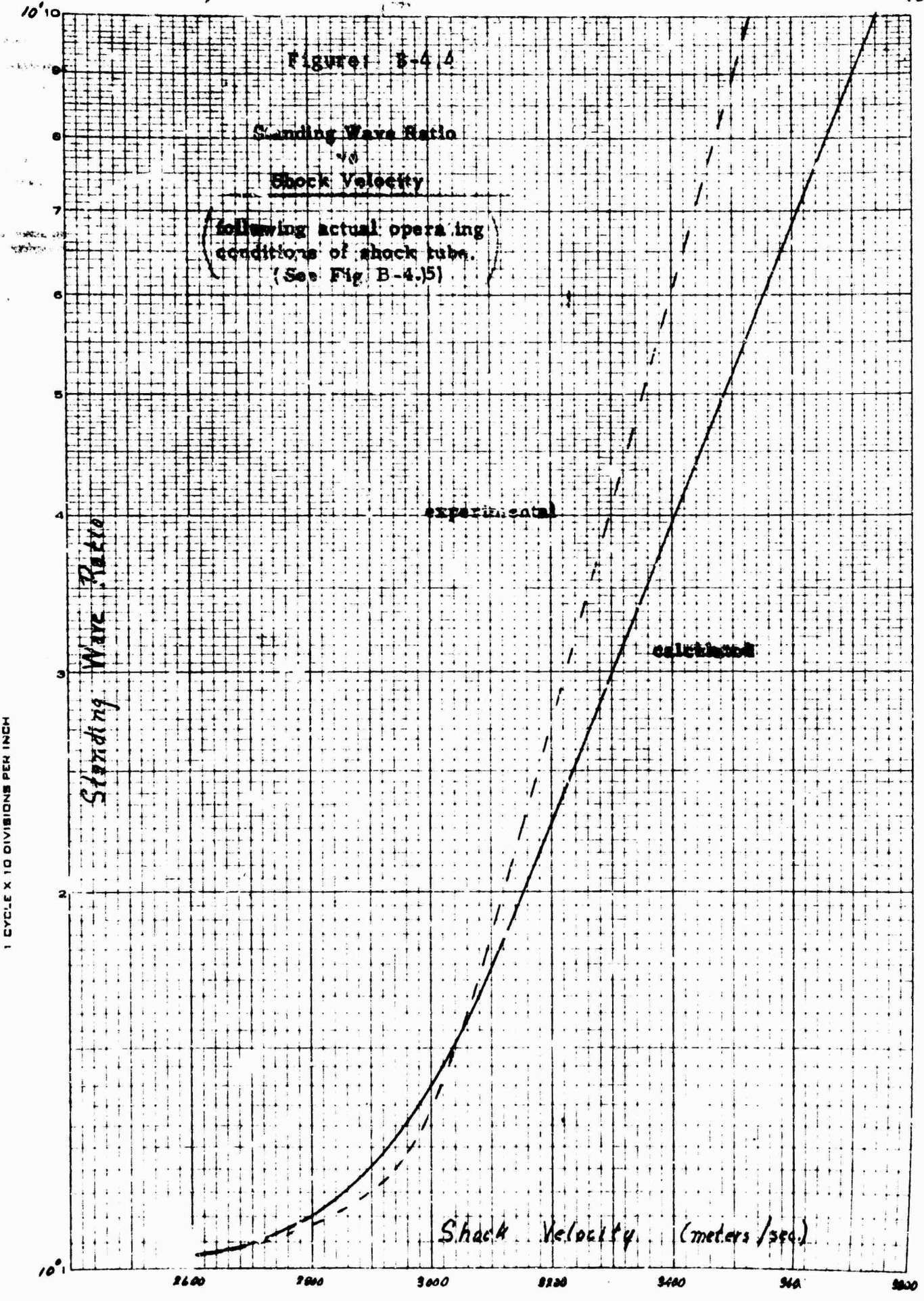

Figure 2-4.2

Spectral Curve

Shock Velocity at Test Section

vs.

Initial Pressure with

Driver 330 psi H_2 at 650°K

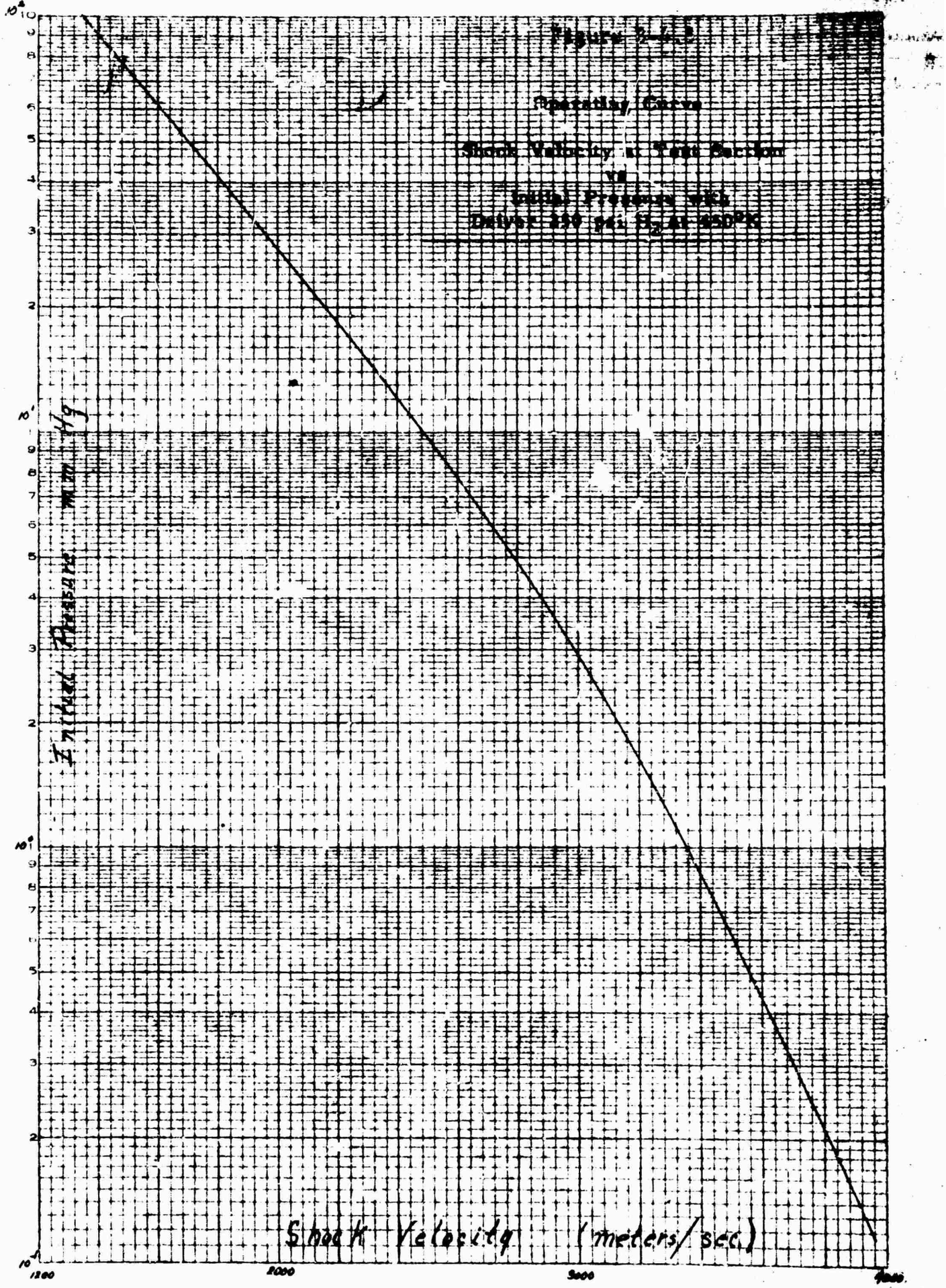

SECT. B-5 RATE CHEMISTRY PROGRAM TO DETERMINE PROPERTIES BEHIND A SHOCK

The following is a brief description of a computer program intended to determine the properties of the flow downstream from a point where all states are specified. Since the parameters which determine the downstream properties are functions of many variables the complete set of equations governing this system must be solved. If the parameters are "rate dependent", then the set must be solved by a step by step procedure. The complexity of this system may be appreciated by realizing that at each step, the chemical reactions of the species (up to 50 reactions and 20 species) must be numerically accounted for, where the concentrations of the species are under the simultaneous effect of other chemical reactions, departures from vibrational equilibrium, and variations in prescribed properties of the flow.

The validity of the result obtained downstream depends on correctness of the assumptions made for the various dynamic processes involved and the numerical constants used to describe the energy states of the species and the rates of reactions.

For the most part, the assumptions used have been satisfactorily verified in other physical regimes. Likewise, the energy states for each species are calculated from "fundamental" data, where the quotation mark means order of magnitude of better accuracy than the error in the calculations. The third set of parameters, the dynamic chemical rate constants, are,

unfortunately, poorly documented.

The difficulty in determining these rate constants is that even for a simple chemical system, a number of reactions can be occurring. At the temperatures and pressures of interest, the relaxation times are generally in the low microsecond region. Compounding this difficulty is that for some species, for example NO, the reaction constants must be established in a complicated environment, where some knowledge of the processes and rates of the other species must be assumed.

This program has been carefully checked for internal consistency and has been checked for the shock conditions for which the important rate constants were deduced. The results for the latter demonstration case are shown in Fig. B-5.1. The relaxation distance for this case corresponds to a fraction of a centimeter behind the shock.

The reactions considered and the rate constants used are given in Appendix I.

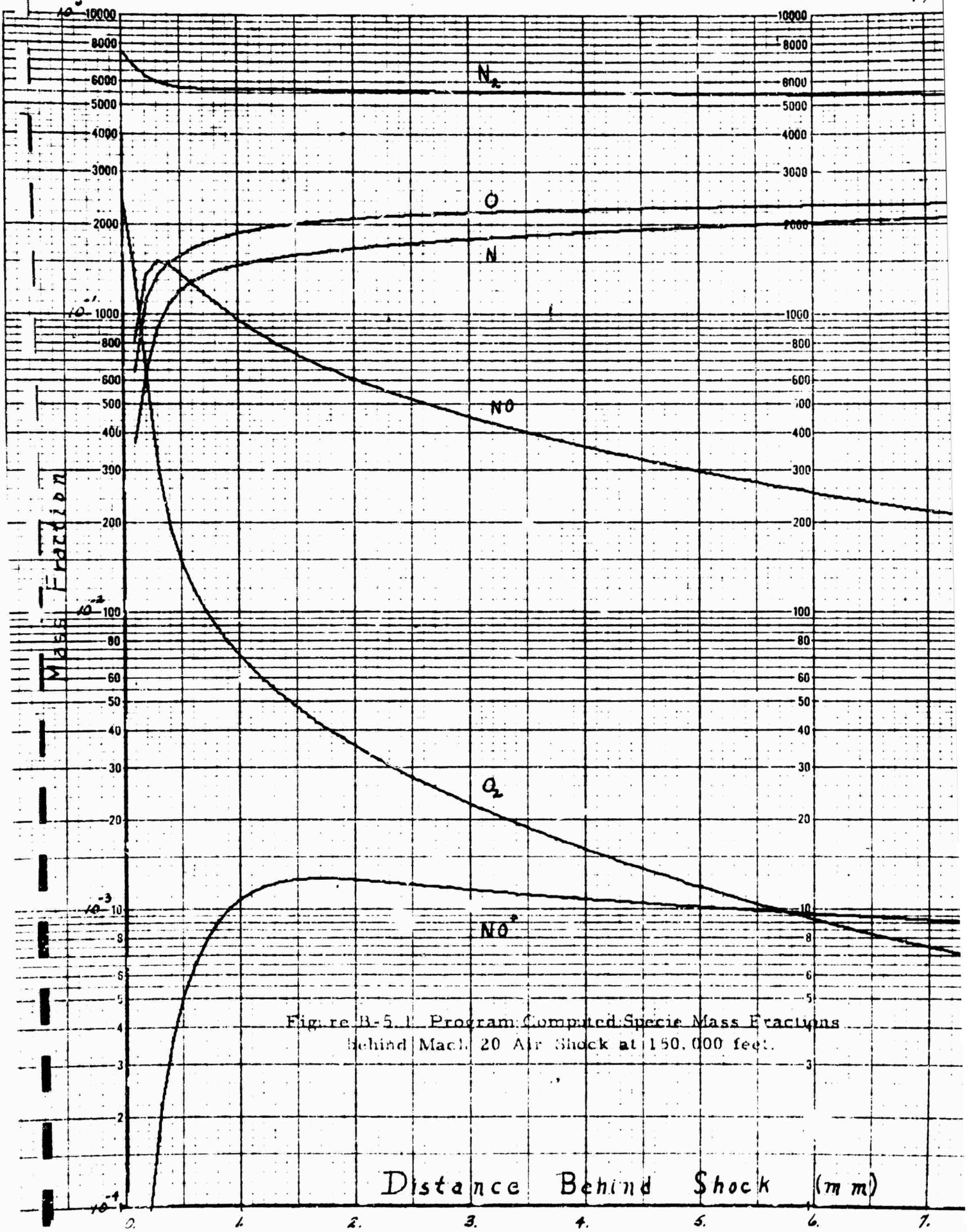

Figure B-5.1 Program Computed Specie Mass Fractions Behind Mach 20 Air Shock at 150,000 feet.

SECT. B-6 COMPARISON BETWEEN EXPERIMENTAL AND COMPUTED ELECTRON DENSITY PROFILE BEHIND MACH 8.9 SHOCK

The basic shock conditions for which this comparison has been made were detailed in Section B-3. The specific velocity and initial pressure correspond to Mach 8.9 shock (3025 m/s) at initial pressure of 134,000 feet altitude (2.0 mm Hg). The curve in Fig. B-6.1 was taken from the "mean" determination discussed in Section B-3.2.

The analytically determined curve in Fig. B-6.1 was calculated from a program similar to that discussed in Section B-5. Actually three separate programs using slightly different procedures and constants have yielded essentially the same curve. The obvious order of magnitude difference in Fig. B-6.1 warrants serious consideration.

Experimentally the checks discussed in Section B-3 have been performed to test the validity of the result. Basically, if an error exists in the experimental information it is either due to the fact that the electron density measuring technique is incorrect or that the plasma is not air alone, but has a contaminant.

The additional measurements discussed in Section B-4 demonstrate quite conclusively that the equilibrium electron density, assuming pure air is used, is achieved in a short distance compared to the waveguide wavelength of the probing microwave frequency. This result is entirely consistent with the point by point measurement. In addition, since the calculation

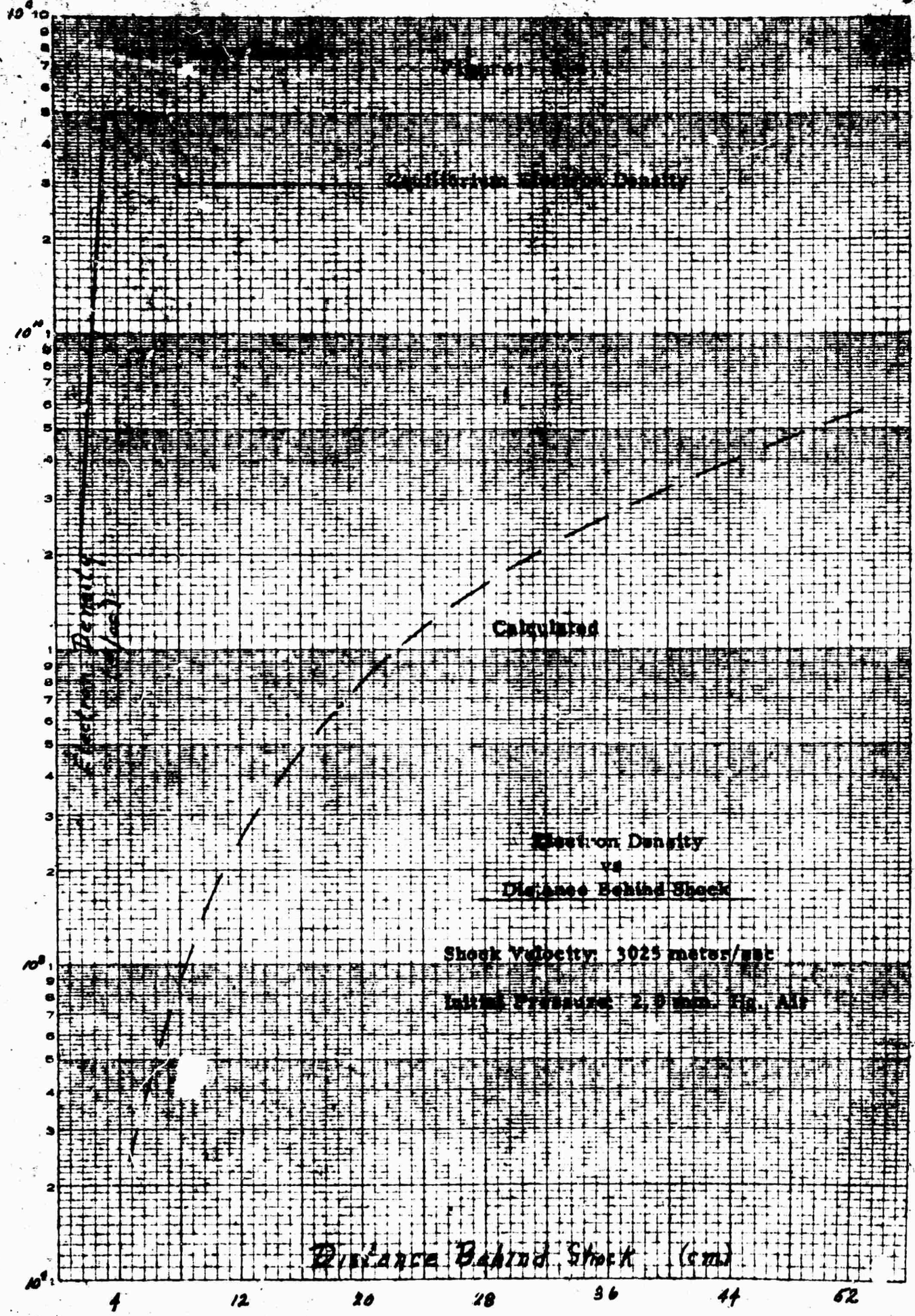
Calculated
Electron Density
vs
Distance Behind Shock
Shock Velocity: 3025 meter/sec
Initial Pressure: 2.9 mm. Hg. Ar
Distance Behind Shock (cm.)
4
12
20
28
36
44
52

of Section B-4 was made assuming a normal air mixture, if an impurity were present, the only reasonable effect it could have would be to act as a catalyst. The rational for this conclusion is that since the difference between the measured and calculated SWR in Fig. B-4.4 corresponds to about 20% in electron density, which is well inside the expected error, any contaminant present does not add significantly to the equilibrium density. If this is so, the contaminant must either act as a catalyst or, by a remarkable coincidence, have the same equilibrium density as air.

If, on the other hand, the error is in the calculated electron density profile, such an error must be effective for the temperature and density conditions pertinent to this shock condition, since the programmed calculation gives satisfactory agreement with experiment for much higher shock Mach numbers.

The obvious location of such an error is in the rate constants. Since it has only recently become possible to alter the rate constants and expression used in the program, no detailed discussion of this work is given here. However, it may be noted that if an error exists in low energy reaction, a compensating error may be present in a high energy reaction. Thus, at high temperature the first error may be undiscernable since the result is principally governed by the higher energy reaction. However, at lower temperatures (recalling that the rate expressions are exponential in nature), the error in the low energy reaction becomes important.

Presented in Fig. B-6.2 are various experimentally determined values for the forward rate constant for the assumed principle ionization process, $NO \rightarrow NO^+ + e$. On this figure, a range of values for this reaction calculated from the properties of the measured profile are given. The range indicated is due to the uncertainty in the other processes. No strong significance should be placed on this initial estimate aside from the fact that it is not inconsistent with the other measured points.

Two basic areas of work are suggested by this result. One is the re-evaluation of the chemical rate processes so as to be consistent with the high and low Mach number conditions. With the new flexible computer program empirical estimated changes can easily be made. Also, a check for an impurity in the air plasma should be made. Such a check can be attempted spectroscopically as discussed in the next section, number B-7.

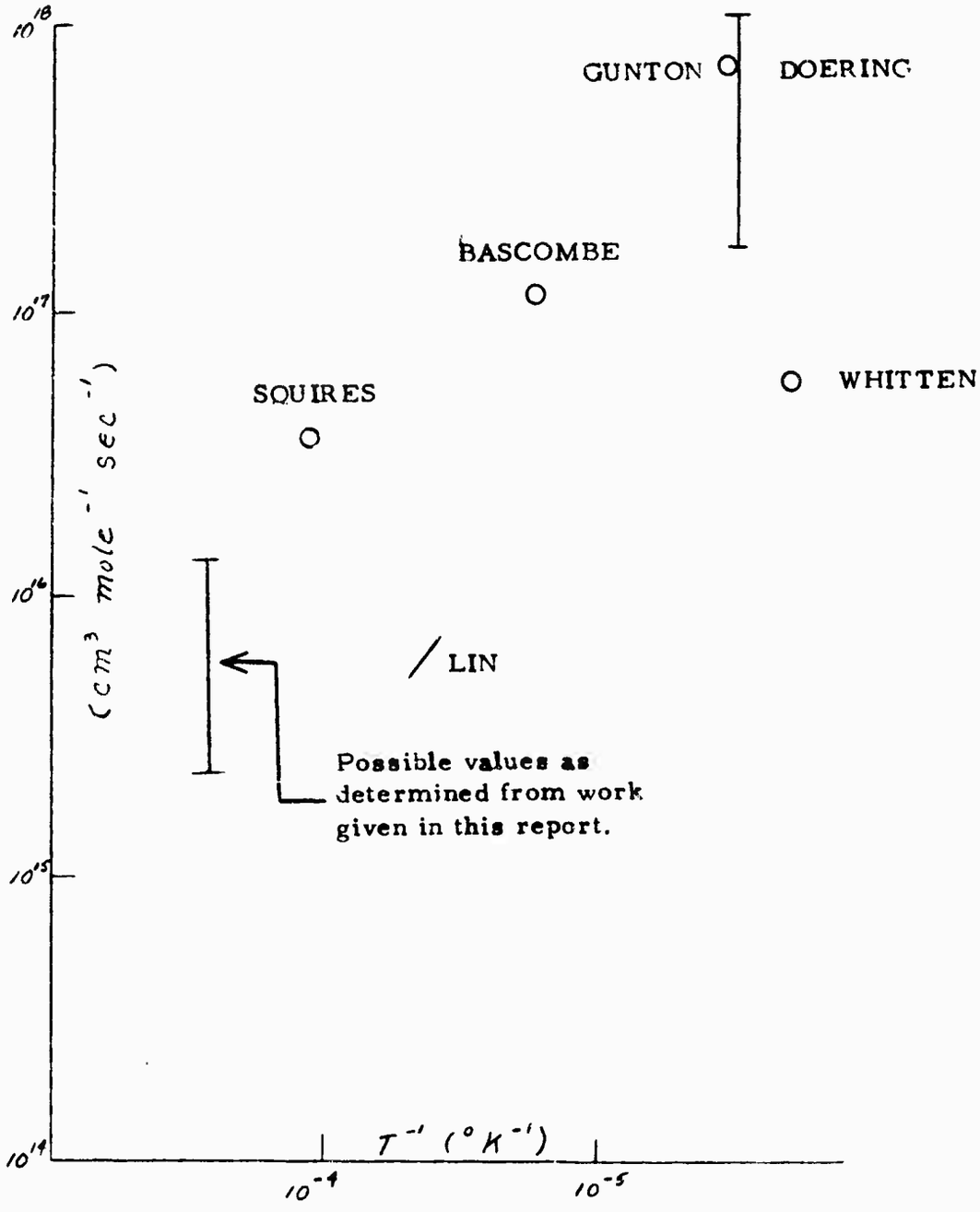

RATE CONSTANT FOR THE REACTION $NO^+ + e \rightarrow N + O$

Figure B-6.2

SECT. B-7 SPECTROSCOPIC SEARCH FOR IMPURITY

In the previous section, it was suggested that one possible "error" in the electron density profile measurement was that an impurity existed in the shock gas which made the result not representative of normal air. Although all possible attempts have been made to minimize impurities (see Section B-3) a persistent criticism of the measurement is the possible existence of an impurity.

To investigate this possibility, a grating spectrometer of large effective aperture has been obtained. (Jerrel Ash model 75-000.) At the time of writing of this report, initial runs are being made using the shock tube.

Extensive calibration of the instrument has been made using an rf-excited discharge tube. This discharge tube was designed so that any given gas or impurity could be introduced and tested at known pressures. While the conditions of this source are not the same as the shock tube, the basic energy levels of the species are, of course, unaltered, even if the relative intensities are dissimilar. Hence, if a specific impurity is suspected, extensive tests can be made to establish its detailed spectra which can then be used to verify or eliminate the existence of such an impurity in the shocked gas spectra.

A subordinate piece of equipment to the spectrograph is a

recording densitometer. A somewhat unique and inexpensive densitometer has been built using the basic parts of the precision enlarging facility used to obtain numerical data from the scope trace.

The spectrographic plate (5x7) is loaded in a modified plate holder for the 3x4 projector. One-half of the seven-inch plate is enlarged about 15 diameters. This enlargement reduces the requirement for high precision stages and slits usually required in such an instrument. At the normal image focal plane, a set of silicon photo cells, one with a slit, is mounted on a precision platform driven by a synchronous motor. At the lens of the projector, a light chopper is used to achieve about 200 cps fluctuation. The use of the fluctuating light source allows the use of narrow band ac amplifiers to increase the output from the photo cells, thus simplifying the design of the amplifiers and minimizing the effects of changes in ambient lighting conditions.

Two photo cells are used, one with a narrow slit (.010") to sample the trace, and the other with no slit (1/4" sq. in area) to sample the unexposed part of the plate. The outputs from the amplifiers for these two photo cells are put in bucking series in a diode detecting circuit. The purpose of the two photo cells is to compensate for changes in "fogging" conditions and remove zero drift due to changes in light intensity. In actual use no discernable drift has been observed even for intensity changes

of a factor of two. The detected compensated output is recorded on a 10" synchronous driven strip recorder.

The overall system from spectrograph to output chart is repeatable to better than .1% enabling an absolute line location to better than 3.0 Å out of 3000 Å, which is twice the minimum resolution of the entire system.

CHAPTER IV

PERIODICALLY DISTURBED PLASMA

SECT. C-1 INTRODUCTION

The simple criterion used to determine radar cross section of an ionized wake is to assume that for electron density regions where $\frac{\omega_p^2}{\omega^2} < 1$, no reflection occurs, and if $\frac{\omega_p^2}{\omega^2} > 1$ total reflection occurs. This simple criteria is useful if the collision frequency is low and the density gradients are large through the above critical conditions.

The problem of interest here is the electromagnetic characteristics of a plasma region where $\frac{\omega_p^2}{\omega^2} \ll 1$, but where stationary or time varying regions of higher density ($\frac{\omega_p^2}{\omega^2}$ still less than 1) occur with spacing comparable to the half wavelength or multiple of the incident radiation. This situation is comparable with a multilayered dielectric filter, except that in general the locations of the maximum electron density regions are randomly changing.

It must be noted that while it is possible to obtain a strong reflection from such a periodic dielectric structure, it is equally probable that total absorption will occur, by the same process. However, if the structure is randomly varying, the process of interest is

that of reflection, which ultimately is detected. The totally absorbed energy is equivalent to a transparent region as far as the reflected characteristics are concerned.

SECT. C-2 EXPERIMENTAL OBSTACLE

In order to properly formulate the analytical model required to generalize the problem, some basic experimental information must be supplied. Of course such information must be sufficiently quantitative that a true model can be formulated. Therein lies the experimental problem, for, since the basic plasma required is strongly underdense, $\left|\frac{\omega_p}{\omega}\right|^2 << 1$, measurement of the plasma properties becomes extremely difficult.

One approach to this measurement problem is to induce the required perturbation in such a manner that the plasma properties can be accurately deduced from other parameters.

One such experimental arrangement considered was to propagate a strong sound wave into the shocked gas. With such an arrangement, the amplitude and spacing of the periodic structure could easily be changed within limits. Since the maximum expected variations in pressure would be small compared to the base pressure, the electron density variation might be assumed to be directly proportional to the pressure variation. That is

$$\frac{\Delta_p}{p} = \frac{\Delta_{ne}}{\bar{n}_e}$$

While all parts of this scheme are correct in concept, severe problems arise in coupling the required sound energy to the shock tube. Although several different coupling systems have been tried, the attempt to use sound waves to induce plasma variations has been abandoned because of the extensive facility that would be required.

To obtain an order of magnitude estimate of the effect of a turbulent wake on the reflected radiation, an experiment was performed in the shock tube. A cylindrical bar was mounted across the tube parallel to the direction of polarization of the radiation. Several diameters were tried up to 1/2", which was the maximum diameter consistent with an unchoked flow. Underdense plasma conditions were run and observations were made of the reflected signal with the use of the electric field detector, in the polarized and antipolarized directions.

Even though the scale of the turbulence expected was an order of magnitude smaller than the wavelength, if very strong effects were to be associated with this type of wake, a noise signal would be imposed on the reflected power signal. Since no such signals were observed, it may be concluded that small scale effects are unimportant in this process.

SECT. C-3 TENTATIVE RESULTS

An attempt was made to see if strong effects could be obtained under conditions where the scale of the disturbance was comparable to the wavelength, even if no precise description of this disturbance could be given.

The basic scheme used was the addition of a "Tee" section to the shock tube, where the area of the arm of the "Tee" is about 1/2 the area of the tube. As the flow passes the "Tee" section, under certain conditions, a "whistle" type effect can occur. If this is the case, periodic pressure fluctuations should be induced in the flow. Such pressure variations should, in turn, create regions of higher electron density.

In figure C-3.1 a trace is presented showing the pressure fluctuations occurring in the arm of the "Tee" near the main flow. Although such variations could only be obtained for a very restricted set of operating conditions, figure C-3.1 clearly shows that some type of periodic pressure producing mechanism is occurring.

To check the validity of the result, a simple step model for the plasma behind the shock can be used to compute the reflected signal. Assuming the pressure defect is carried with the flow, the simple model for the plasma postulates a reflection from the front

of the shock and a second reflection from the pressure disturbed region which exists behind the shock a distance (z) where $z = v_o t$ with v_o the particle velocity with respect to the shock and time t starting from the creation of the disturbance.

For the moment, if it is assumed that the waveguide wavelength is not appreciably altered in the first plasma region directly behind the shock, then it is clear that when the distance $z = \frac{\lambda_g}{4}$, the reflected signal from the disturbed region will be 180^o out of phase from the reflection occurring at the front of the shock, thus producing a minimum in the standing wave ratio. On the other hand, for $z = \lambda g/2$ the two reflected signals are in phase and a maximum should occur in the SWR.

In figure C-3.2 a trace of the electric field is shown for the critical whistle conditions described. While this result must be considered tentative, it is clear that before the shock enters the "Tee" section, the SWR is small indicating an "underdense" plasma. After the transition of the "Tee" where the effects cannot be clearly described at the present time, the amplitude modulation of the SWR is seen to decrease and then subsequently to increase. The end transition occurs as first the plasma passes the detector and then

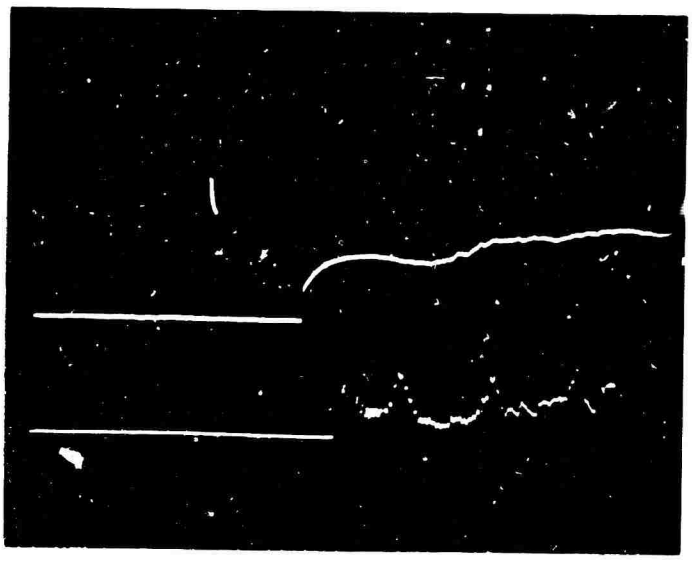

Top Trace: Heat transfer gauge located at entrance to "Tee" section.

Lower Trace: Pressure in arm of "Tee".

Sweep Time: 100 μs/cm.

Figure C-3.1

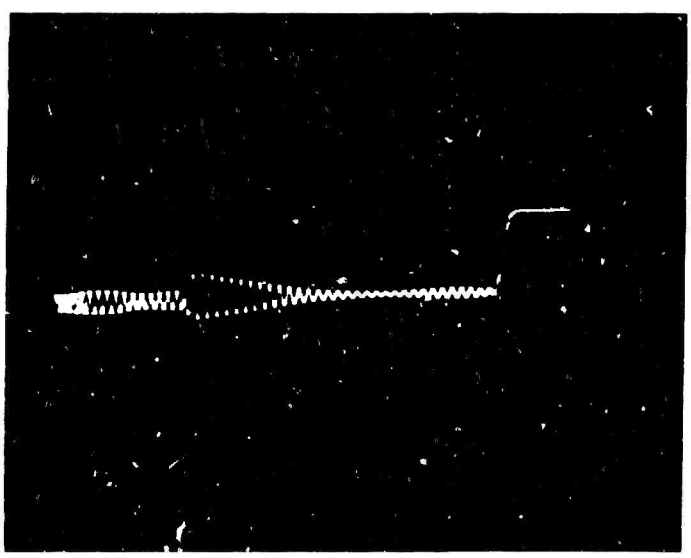

Electric Field Detector. Located 3 meters downstream of "Tee" section.

Sweep Time: 200 μs/cm.

Note: The cancellation and subsequent growth of the signal as the "filter" structure goes through the $\frac{\lambda_g}{4}$ condition.

Figure C-3.2

reaches the antenna, where the signal drops to zero. Since this type of modulating behavior is consistent with the simple model and inconsistent with other possible mechanisms, it is felt that this trace represents the type of strong reflections that can be obtained.

REFERENCES

1. Tamagno, J. and Palatnik, A., Instrumentation Techniques for Heat Transfer Measurement in Hypersonic Shock Tunnel, GASL TM-102, January 1964

2. Lin, S. C., Rate of Ionization Behind Shock Waves in Air, AVCO Research Note 170, 1959.

3. Whitten, R. C. and Poppoff, I. G., J. Geophys. Res., 66, 2779, 1961.

4. Squires, B. E., Jr., Pennsylvania State Univ. Ionospheric Research Scientific Rpt. No. 144, 1961.

5. Bascombe, K., Jenkins, D., Schiff, H. I., and Sugden, T. M., 9th Annual Conference on Mass Spectrometry, Chicago, June 1961.

6. Gunton, R. C. and Inn, E. C. Y., J. Chem. Phys. 35, 1896, 1961.

APPENDIX I

SUMMARY OF CHEMICAL REACTIONS AND THEIR RATE CONSTANTS[1]

This appendix summarizes a large number of chemical reactions which are significant at the high temperatures of reentry into the earth's atmosphere at hypersonic speeds. In all cases the data was taken from the survey of Steiger,[2] and the original sources may be found in this reference.

The presentation here includes two classes of units, namely cm, sec, particle (used in Reference 2) and meter, sec, kg mole (required for the present analysis). The tables are self-explanatory, though a word of caution is in order for the ionization reactions 10 through 15. The rate constants for these reactions are tabulated as the forward (i.e. to the right) values, which is contrary to the remainder of the appendix.

---

[1] Gavril, B. D., Generalized One-Dimensional Chemically Reacting Flows with Molecular Vibrational Relaxation, GASL Technical Report No. 426, January 29, 1964.

[2] Steiger, M. H., On the Chemistry of Air at High Temperatures, GASL Technical Report No. 357, June 17, 1963.

SUMMARY OF CHEMICAL REACTIONS AND RATE CONSTANTS

No. j	REACTION	CATALYST X	n	REVERSE RATE CONSTANT AT EQUILIBRIUM $(k^x_{j-})_e$		Reference
				$\frac{\text{kg moles}}{\text{m}^3\text{sec}}\left(\frac{\text{m}^3}{\text{kg mole}}\right)^n$	$\frac{\text{particles}}{\text{cm}^3\text{sec}}\left(\frac{\text{cm}^3}{\text{particle}}\right)^n$	
1	$O_2 + X + 5.1\ ev = 2O + X$	O	3	$2.3 \times 10^{14}\ T^{-3/2}$	$6.2 \times 10^{-28}\ T^{-3/2}$	
		O_2		$8.0 \times 10^{13}\ T^{-3/2}$	$2.2 \times 10^{-28}\ T^{-3/2}$	
		N_2		$6.2 \times 10^{9}\ T^{-1/2}$	$1.7 \times 10^{-32}\ T^{-1/2}$	
		all other		$3.0 \times 10^{9}\ T^{-1/2}$	$8.3 \times 10^{-33}\ T^{-1/2}$	
2	$N_2 + X + 9.8\ ev = 2N + X$	N	3	$2.4 \times 10^{15}\ T^{-3/2}$	$6.5 \times 10^{-27}\ T^{-3/2}$	
		N_2		$2.8 \times 10^{10}\ T^{-1/2}$	$7.6 \times 10^{-32}\ T^{-1/2}$	
		all other		$1.1 \times 10^{10}\ T^{-1/2}$	$3.0 \times 10^{-32}\ T^{-1/2}$	

SUMMARY OF CHEMICAL REACTIONS AND RATE CONSTANTS

No. j	REACTION	CATALYST X	n	REVERSE RATE CONSTANT AT EQUILIBRIUM $(k^x_{j-})_e$		Reference
				$\frac{\text{kg moles}}{\text{m}^3\text{sec}}\left(\frac{\text{m}^3}{\text{kg mole}}\right)^n$	$\frac{\text{particles}}{\text{cm}^3\text{sec}}\left(\frac{\text{cm}^3}{\text{particle}}\right)^n$	
3	$NO + X + 6.5\ ev = N + O + X$	A	3	$1.7 \times 10^{14}\ T^{-3/2}$	$4.66 \times 10^{-28}\ T^{-3/2}$	
		NO		$2.0 \times 10^{15}\ T^{-3/2}$	$5.5 \times 10^{-27}\ T^{-3/2}$	
		all other		$1.0 \times 10^{14}\ T^{-3/2}$	$2.8 \times 10^{-28}\ T^{3/2}$	
4	$O + N_2 \quad 3.3\ ev = NO + N$		2	1.6×10^{10}	2.7×10^{-11}	
5	$NO + O + 1.4\ ev = N + O_2$		2	$1.3 \times 10^{7}\ T \exp\left(-\frac{3560}{T}\right)$	$2.2 \times 10^{-14}\ T \exp\left(-\frac{3560}{T}\right)$	
6	$N_2 + O_2 \quad 1.9\ ev = 2NO$		2	$2.4 \times 10^{20}\ T^{-5/2} \exp\left(-\frac{43{,}000}{T}\right)$	$0.4 \times T^{-5/2} \exp\left(-\frac{43{,}000}{T}\right)$	

SUMMARY OF CHEMICAL REACTIONS AND RATE CONSTANTS

No. j	REACTION	CATALYST X	n	REVERSE RATE CONSTANT AT EQUILIBRIUM $\left(\frac{1^x}{Kj-}\right)_e$		Reference
				$\frac{\text{kg moles}}{m^3 \text{sec}} \left(\frac{m^3}{\text{kg mole}}\right)^n$	$\frac{\text{particles}}{cm^3 \text{sec}} \left(\frac{cm^3}{\text{particle}}\right)^n$	
7	$N + O + 2.8\ ev = NO^+ + e^-$		2	$1.8 \times 10^{18}\ T^{-3/2}$	$3 \times 10^{-3}\ T^{-3/2}$	
8	$2N + 5.8\ ev = N_2^+ + e^-$		2	$1.8 \times 10^{18}\ T^{-3/2}$	$3 \times 10^{-3}\ T^{-3/2}$	
9	$2O + 6.9\ ev = O_2^+ + e^-$		2	$1.2 \times 10^{18}\ T^{-3/2}$	$2 \times 10^{-3}\ T^{-3/2}$	

SUMMARY OF CHEMICAL REACTIONS AND RATE CONSTANTS

No. j	REACTION	CATALYST X	n	FORWARD RATE CONSTANT AT EQUILIBRIUM $(k^x_{j+})_e$		Reference
				* $\frac{\text{kg moles}}{\text{m}^3\text{sec}}\left(\frac{\text{m}^3}{\text{kg mole}}\right)^n$	** $\frac{\text{particles}}{\text{cm}^3\text{sec}}\left(\frac{\text{cm}^3}{\text{particle}}\right)^n$	
10	$X + NO + 9.3\,ev = X + NO^+ + e^-$	all species	2	$\left.\begin{matrix}2.7\times10^{-4}\\4.5\times10^{-25}\end{matrix}\right\} T^{5/2}\,(1+3\times10^{-5}T)\exp\left(-\frac{107,900}{T}\right)$		* = upper content of brace
11	$N_2 + O_2 + 11.2\,ev = NO + NO^+ + e^-$		2	$\left.\begin{matrix}2.7\times10^{-4}\\4.5\times10^{-25}\end{matrix}\right\} T^{5/2}\,(1+3\times10^{-5}T)\exp\left(-\frac{141,000}{T}\right)$		** = lower content of brace
12	$X + O_2 + 12.1\,ev = X + O_2^+ + e^-$	N_2	2	$\left.\begin{matrix}2.7\times10^{-4}\\4.5\times10^{-25}\end{matrix}\right\} T^{5/2}\,(1+3\times10^{-5}T)\exp\left(-\frac{141,000}{T}\right)$		
		O_2	2	$\left.\begin{matrix}6.6\times10^{-13}\\1.1\times10^{-33}\end{matrix}\right\} T^{9/2}\,(1+4\times10^{-5}T)\exp\left(-\frac{141,000}{T}\right)$		
		all other	2	use value for N_2		
13	$X + O + 13.6\,ev = X + O^+ + e^-$	all species	2	$\left.\begin{matrix}2.7\times10^{-4}\\4.5\times10^{-25}\end{matrix}\right\} T^{5/2}\,(1+3\times10^{-5}T)\exp\left(-\frac{157,000}{T}\right)$		

SUMMARY OF CHEMICAL REACTIONS AND RATE CONSTANTS

No. j	REACTION	CATALYST X	n	FORWARD RATE CONSTANT AT EQUILIBRIUM $\left(k^{x}_{j+}\right)_e$	Reference
				* $\frac{\text{kg moles}}{\text{m}^3\text{sec}}\left(\frac{\text{m}^3}{\text{kg mole}}\right)^n$ | ** $\frac{\text{particles}}{\text{cm}^3\text{sec}}\left(\frac{\text{cm}^3}{\text{particle}}\right)^n$	
14	$X + N + 14.6\ ev = X + N^+ + e^-$	all species	2	$\left.\begin{matrix}2.7\times10^{-4}\\ 4.5\times10^{-25}\end{matrix}\right\} T^{5/2}\left(1+3\times10^{-5}T\right)\exp\left(-\frac{169,400}{T}\right)$	* = upper content of brace
15	$X + N_2 + 15.6\ ev = X + N_2^+ + e^-$	N_2 and all other	2	$\left.\begin{matrix}1.7\times10^{-7}\\ 2.8\times10^{-28}\end{matrix}\right\} T^{7/2}\left(1+3\times10^{-5}T\right)\exp\left(-\frac{181,000}{T}\right)$	** = lower content of brace

SUMMARY OF CHEMICAL REACTIONS AND RATE CONSTANTS

No. j	REACTION	CATALYST X	n	REVERSE RATE CONSTANT AT EQUILIBRIUM $\left(k^{x}_{j-}\right)_e$		Reference
				$\frac{\text{kg moles}}{\text{m}^3\text{sec}}\left(\frac{\text{m}^3}{\text{kg mole}}\right)^n$	$\frac{\text{particles}}{\text{cm}^3\text{sec}}\left(\frac{\text{cm}^3}{\text{particle}}\right)^n$	
16	$N + O_2^+ + 0.2\,ev = O^+ + NO$		2	$7.8\times10^{8}\ T^{1/2}$	$1.3\times10^{-12}\ T^{1/2}$	
17	$NO + NO^+ + 0.9\,ev = N_2 + O_2^+$			for all reactions on this page		
18	$N + O^+ + 0.9\,ev = N^+ + O$					
19	$N_2 + N^+ + 1.0\,ev = N_2^+ + N$					
20	$NO^+ + N + 1.1\,ev = N_2 + O^+$					
21	$O + O_2^+ + 1.6\,ev = O^+ + O_2$					
22	$N_2 + O^+ + 2.0\,ev = N_2^+ + O$					
23	$O + N_2^+ + 2.2\,ev = N^+ + NO$					
24	$NO + O^+ + 2.3\,ev = O_2 + N^+$					
25	$N + O_2^+ + 2.5\,ev = N^+ + O_2$					

SUMMARY OF CHEMICAL REACTIONS AND RATE CONSTANTS

No. j	REACTION	CATALYST X	n	REVERSE RATE CONSTANT AT EQUILIBRIUM $(k_{j-}^{x})_e$		Reference
				$\frac{\text{kg moles}}{\text{m}^3\text{sec}}\left(\frac{\text{m}^3}{\text{kg mole}}\right)^n$	$\frac{\text{particles}}{\text{cm}^3\text{sec}}\left(\frac{\text{cm}^3}{\text{particle}}\right)^n$	
26	$O_2 + NO^+ + 2.8\ ev = O_2^+ + NO$		2	$7.8\times10^{8}\ T^{1/2}$	$1.3\times10^{-12}\ T^{1/2}$	
27	$NO^+ + N + 3.1\ ev = N_2^+ + O$			for all reactions on this page		
28	$N_2 + O_2^+ + 3.5\ ev = N_2^+ + O_2$					
29	$NO^+ + C + 4.2\ ev = O_2^+ + N$					
30	$N_2 + O^+ + 4.2\ ev = NO + N^+$					
31	$O + NO^+ + 4.4\ ev = O^+ + NO$					
32	$NO + NO^+ + 4.5\ ev = N_2^+ + O_2$					
33	$N + NO^+ + 5.3\ ev = N^+ + NO$					
34	$N_2 + NO^+ + 6.3\ ev = N_2^+ + NO$					
35	$NO^+ + O + 6.7\ ev = O_2 + N^+$					

SUMMARY OF CHEMICAL REACTIONS AND RATE CONSTANTS

No. j	REACTION	CATALYST X	n	REVERSE RATE CONSTANT AT EQUILIBRIUM $\left(k_{j-}^{x}\right)_e$		Reference
				$\frac{\text{kg moles}}{\text{m}^3\text{sec}}\left(\frac{\text{m}^3}{\text{kg mole}}\right)^n$	$\frac{\text{particles}}{\text{cm}^3\text{sec}}\left(\frac{\text{cm}^3}{\text{particle}}\right)^n$	
36	$X + O^- + 1.465\ ev = X + O + e^-$	all species	3	$1.1\times10^{13} T^{-1}$	$3.03\times10^{-29} T^{-1}$	
37	$X + O_2^- + 0.46\ ev = X + O_2 + e^-$	O_2	3	$3.1\times10^{14} T^{-1}$	$8.4\times10^{-28} T^{-1}$	
		all other		$7.6\times10^{12} T^{-1}$	$2.1\times10^{-29} T^{-1}$	
38	$NO + O + 7.835\ ev = O^- + NO^+$		2	$1.0\times10^{15} T^{-1/2}$	$1.7\times10^{-6} T^{-1/2}$	
39	$NO + O_2 + 8.84\ ev = O_2^- + NO^+$		2	$1.0\times10^{15} T^{-1/2}$	$1.7\times10^{-6} T^{-1/2}$	